Monte Carlo analysis of methods for extracting risk-neutral densities with affine jump diffusions

Shan Lu

School of Management
University of Bradford
Emm Lane, Bradford
BD9 4JL, UK

Tel: +44 (0)1274 238101
Email: s.lu4@bradford.ac.uk

Acknowledgement:
I thank the editor, Robert Webb, and an anonymous referee for helpful comments and suggestions. I also thank Naveed Khan for providing a detailed guidance on the Maxwell cluster at the University of Aberdeen where simulations were run and completed.

Monte Carlo analysis of methods for extracting risk-neutral densities with affine jump diffusions

Abstract

This paper compares several widely-used and recently-developed methods to extract risk-neutral densities (RND) from option prices in terms of estimation accuracy. It shows that positive convolution approximation method consistently yields the most accurate RND estimates, and is insensitive to the discreteness of option prices. RND methods are less likely to produce accurate RND estimates when the underlying process incorporates jumps and when estimations are performed on sparse data, especially for short time-to-maturities, though sensitivity to the discreteness of the data differs across different methods.

Keywords: Risk-neutral density; Monte Carlo simulation; Affine jump diffusions.

1. Introduction

This paper compares the performance of various estimation methods to extract risk-neutral densities (RND) from option prices. Since the true RND is latent, a pseudo-price based methodology is used to evaluate the performance of the RND methods in terms of estimation accuracy and consistency. The pseudo-based method begins with an assumed affine jump diffusion model and a set of estimated model parameters, the hypothetical affine jump diffusion model is then used to generate artificial option data by using the model parameters; the 'true' RND is obtained analytically from the model according to the result of Breeden and Litzenberger (1978), whereas the RND estimate is extracted by RND methods from the artificial option data. The performance of the RND methods is then tested by comparing the 'true' RND and the RND estimate through a goodness-of-fit test. The procedure is repeated for 1000 times in order to provide the distributional information about the test statistic, which answers the question of how likely these RND methods produce statistically accurate estimates in practice. The procedure is repeated for artificial option data with different maturities.

The study differs from prior research on the comparison of RND methods in several aspects of the methodology. Firstly, the assumed hypothetical underlying process for price and volatility takes both price and volatility jumps into consideration, making the comparison more realistic than prior comparison studies do, though no-jump and single-jump models are also employed for comparison purposes. Most prior studies on the comparison of RND methods assume either a single parametric form of the RND or a stochastic process of the underlying asset price and volatility. For example, Söderlind (2000) start with an assumed parametric form of the RND, and employ a Monte Carlo simulation to fit option prices based on the assumed error distribution; Bu and Hadri (2007); Santos and Guerra (2015) start with the Heston model. Furthermore, in the case of assuming stochastic processes for the underlying asset price and volatility, prior studies assume stochastic volatility processes that account for either no jumps or only price jumps (Lai, 2014; Santos and Guerra, 2015),

and no prior studies have employed the double-jump model for the comparison of RND methods. It should be noted that the inclusion of both price and volatility jumps in the hypothetical underlying asset process is consistent with the findings in equity price dynamics and option pricing literature. For example, Broadie, Chernov, and Johannes (2007) find strong evidence of the presence of both price and volatility jumps in time series of equity prices, and both jumps are important components for option pricing. Secondly, we adopt a noise perturbation procedure proposed by Bondarenko (2003a) which is consistent with the options exchange's regulation on maximum bid-ask differentials to simulate the market frictions such as the bid-ask spread; whereas prior studies do not consider the regulation on maximum bid-ask differentials when adding noises to the simulated option prices: for example, Lai (2014) sets the price noise to be a proportional white noise to the simulated option prices; Bliss and Panigirtzoglou (2002); Santos and Guerra (2015) add an uniformly distributed random noise whose size is between minus half and half of the option price tick size.

Eight RND methods compared in this study consist of both parametric and nonparametric, widely-used and recently developed methods, spanning a wide range of categories of methods. These methods include: mixture of two lognormals (LN2) (Ritchey, 1990), hermite polynomial with Gram-Charlier expansion (HPGC) (Jondeau and Rockinger, 2001), generalized beta distribution of the second kind (GB2) (Bookstaber and MacDonald, 1987), generalized extreme value distribution (GEV) (Markose and Alentorn, 2011), curve-fitting with quadratic polynomial (QP) (Shimko, 1993), curve-fitting with cubic smoothing spline (CS) (Bliss and Panigirtzoglou, 2004), positive convolution approximation (PCA) (Bondarenko, 2000, 2003a) and spectral recovery method (SRM) (Monnier, 2013).

The evaluation of estimation methods for RNDs is important for both market participants and policymakers, since RNDs embedded in option prices have important financial and economic applications. Risk preferences of market agents embedded in RNDs play important roles in the modelling and determination of insurance policies, pension plans and tax

regulations. Higher moments of RNDs contain predictive content about stock returns and returns of option portfolios (Bali and Murray, 2013). Policymakers use RND estimates to access the credibility of monetary policy (Bahra, 2007; Olijslagers, Petersen, de Vette, and van Wijnbergen, 2018), gauge market sentiment and access market beliefs about economic and political events (e.g. Birru and Figlewski, 2012). Option traders over-the-counter rely on RND estimates to price exotic options. In addition, RNDs are also used to test market rationality (Bondarenko, 2003b), access bankruptcy probabilities of financial institutions (Taylor, Tzeng, and Widdicks, 2014), measure risk premiums (Ivanova and Gutiérrez, 2014) and study volatility pricing kernels (Völkert, 2015).

We find that, firstly, PCA consistently yields the most accurate RND estimates and is insensitive to the discreteness of option prices, whereas the LN2 method performs the worst. HPGC is the best performer among parametric methods; both HPGC, GB2 and GEV in the parametric domain outperforms the QP in the nonparametric domain. Secondly, RND methods are less likely to produce accurate RND estimates when the underlying process incorporates jumps, especially for short time-to-maturities. Thirdly, the discreteness of option prices negatively affects most RND methods, especially for the short time-to-maturities and when the generating process incorporates double jumps, though sensitivity to the discreteness of the data differs across different methods. Lastly, double-jump models outperform models with no jumps or single-jump models, reinforcing the finding in the equity price dynamics and option pricing literature that both price and volatility jumps are important components for option pricing.

The rest of the paper is organized as follows: Section 2 reviews the RND methods in the literature and briefly introduces and discusses the methods compared in the paper. Section 3 presents the affine jump diffusion models and the model-derived RND functions. Section 4 presents the data. The methodologies for the analysis of RND methods are presented in Section 5. Section 6 presents the results. Section 7 concludes the paper.

2. Literature Review

2.1. RND Methods

Numerous methods to extract RNDs from option prices have been developed (See, Jackwerth, 1999, 2004; Figlewski, 2018, for a review). There are mainly two strands of methods: parametric and nonparametric methods. On the one hand, parametric methods fit the RND to a parametric form of selected densities; they often estimate the parameters by minimizing the sum of pricing errors. Nonparametric methods, on the other hand, directly estimate the RND from linear/nonlinear segments or by pointwise fitting. Compared to parametric methods which assume a functional form of distributions, nonparametric methods are data-driven and more flexible.

There are three major categories within parametric methods: the Mixture methods, the Expansion methods, and the Generalized distribution methods. Mixture methods use the weighted averages of several simple distributions to add flexibility to the estimated probability distribution. A typical example is the mixture of two lognormal distributions (Ritchey, 1990). The problem with the mixture methods is data overfitting which leads to estimated densities with erratic spikes. Expansion methods use a simple standard distribution as the base distribution, and adds correction terms to the base distribution via extra functions such as the confluent hypergeometric functions (Abadir and Rockinger, 2003); Hermite polynomials (Xiu, 2014); the Gram-Charlier expansion (Jondeau and Rockinger, 2001). A common problem with the expansion methods is that the estimated distribution are not guaranteed to always be positive and integrates to 1. Generalized distribution methods often use a flexible distribution or a family of distributions; these distributions are more flexible than the standard Gaussian distributions, and allow skewness and kurtosis to vary, thereby having the ability to describe leptokurtic properties of the distribution of financial data. Examples of generalized distributions include Beta function of the second kind (Bookstaber and MacDonald, 1987); Burr-type distributions (Sherrick, Irwin, and Forster, 1996); and the Generalized

extreme value distribution (Markose and Alentorn, 2011).

There are roughly three major categories within the nonparametric domain: the Kernel method, the Maximum entropy method, and the curve-fitting method. The kernel method usually fits a function to option prices or implied volatility curve; these functions are assumed to pass by all the data points with a kernel measuring the likelihood of the function passing by the data points; the bandwidth of the kernel controls the smoothness of the estimated densities; the choice of the kernel is often the standard normal distribution. Specific kernel methods include the Kernel regression (Aït-Sahalia and Lo, 1998); the Kernel convolution (Bondarenko, 2000, 2003a); and nonparametric least squares (Hardle and Yatchew, 2002). A typical problem with the kernel methods is that they are unable to fit a smooth function to option data with strike price exhibiting gaps. The maximum entropy method estimates the risk-neutral density by maximizing the cross-entropy of logarithmic ratios of the posterior risk-neutral density to a prior density; the method requires the least amount of information about the prior density; the choice of the prior density is often the lognormal distribution. They are developed with different specifications of the prior probability distribution (see e.g. Rockinger and Jondeau, 2002). The curve-fitting method estimates the risk-neutral density by fitting a function of the implied volatilities, and proceeding with the lines of Breeden and Litzenberger (1978); most curve-fitting practice uses fitting criteria such as minimizing the sum of pricing errors or the squared differences in implied volatilities. Examples include splines (Andersen and Wagener, 2002); Polynomial (Shimko, 1993; Rosenberg and Engle, 2002); and smoothing pointwise implied volatilities (Jackwerth, 2000). Besides, in a departure to the three aforementioned categories within the nonparametric methods domain, and in association of this study, Monnier (2013) proposes a method based on the spectral decomposition.

In addition to parametric and nonparametric methods, there are some other methods proposed. Structural models such as the Heston model assume a specific form of the underlying process for price and volatility; the risk-neutral density is estimated numerically by

taking the second derivative of the call price function. Implied trees are a discretization of a single-dimensional diffusion process where volatility is a function of time; the risk-neutral probabilities are obtained numerically for the terminal stock prices (Derman and Kani, 1994). Moreover, Eriksson, Ghysels, and Wang (2009) propose a method based on the empirical risk-neutral moments; Garcia, Lewis, Pastorello, and Renault (2011) propose a method based on moments of integrated volatility; Ross (2015) propose a method that separates objective and risk-neutral densities directly from option prices.

2.2. Methods Compared

The RND methods compared in this paper are summarized in Table 1. Each of the methods belong to a particular category of the RND methods; RND methods are selected according to the following criteria: (1) widely-used methods (2) recently-developed methods; (3) methods that are of less computational complexity. Below is a brief introduction to each of the methods.

[Insert Table 1 around here]

The mixture of two lognormal distributions (LN2) method of Ritchey (1990) estimates the RND by a weighted combination of two lognormal distributions. The mixture of lognormal densities imply that the method assumes option prices are a mixture of Black-Scholes prices.

Hermite Polynomial with Gram-Charlier Expansion (HPGC) method of Jondeau and Rockinger (2001) is based on the Gram-Charlier expansion. The method relies on the Hermite polynomial approximation of Abken, Madan, and Ramamurtie (1996) with additional constraints added to the third and forth moments of estimated RND. The advantage of this method over other methods using the Hermite polynomial is that the additional constraints ensure the positivity of the density estimates.

The generalized beta distribution of the second kind (GB2) of Bookstaber and MacDonald (1987) is applied to the estimation of RND by Anagnou, Bedendo, Hodges, and Tompkins

(2002); Taylor (2005); Liu, Shackleton, Taylor, and Xu (2007). The method assumes the RND to be in a parametric form of GB2. The GB2 distribution is a generalized distribution which nests some common types of distributions such as the lognormal, Burr type, Weibull and exponential distributions. Therefore, the shape of the estimated RND is more flexible than that estimated from the LN2.

Markose and Alentorn (2011) proposes a method by assuming the parametric form of the risk-neutral distribution to be the Generalized extreme value distribution (GEV), and develops the closed-form solutions for European call and put option prices for the GEV-based risk-neutral distribution function; the parameters of the GEV distribution are estimated by minimizing the option pricing errors. The GEV method has the advantage over the LN2 method that the shape of RND estimates obtained from the GEV method is more flexible, and GEV provides with the ability to fit long-tailedness of the distribution of financial prices whereas LN2 doesn't have the capacity.

The basic idea of the quadratic polynomial (QP) method of Shimko (1993) is to use the Black-Scholes formula to transform option prices into the implied volatility space, and then fit a quadratic polynomial to back out the entire implied volatility curve, the RND can then be obtained analytically. However, it is suggested that the implied volatility smile may exhibit different levels of curvature depending on the market conditions (e.g. Rubinstein, 1994); and if the implied volatility smile exhibits pronounced skew, then the quadratic function is likely not suitable for fitting the implied volatility simile (Aparicio and Hodges, 1998), and could lead to negative risk-neutral probabilities.

Bliss and Panigirtzoglou (2004) proposes to fit a vega-weighted cubic smoothing spline to the implied volatility in the delta space, with a smoothing parameter which controls the trade-off between the goodness-of-fit and the smoothness of the fitted RND. Vega weighting has the advantage of placing more weights on the near-the-money options, which is consistent with the high liquidity of such options. And smoothing implied volatilities in the delta space allows a greater flexibility in the shape of the estimated RND especially near the center of

the distribution (Malz, 1997).

The basic idea of the positive convolution approximation (PCA) method of Bondarenko (2000, 2003a) is to select an optimal density that best fits the observed option prices from a set of candidate densities. Specifically, Bondarenko (2000, 2003a) approximate the RND by the weights of a linear combination of normal densities with the linear combination being fitted to a cross section of put option prices. The advantage of the PCA method is that it minimizes the possible overfitting. And it is suggested in the literature that the good performance of kernel methods is attributed to their ability to discount the effect of outliers in the noisy data (Lai, 2014).

The basic idea of the spectral recovery method (SRM) of Monnier (2013) is to find the smoothest RND that satisfies no-arbitrage and bid-ask constraints from a set of valid equivalent RNDs implied by bid and ask quotes of put options. The SRM views the RND estimation as an inverse problem. It first defines a framework of restricted put and call operators that admit a singualr value decomposition, and the framework subsequently allows one to adopt a quadratic programming method to extract the smoothest RND whose put prices satisfy the bid-ask constriants.The advantage of the SRM method is that it gives the entire left tail of the RND, given the fact that the market exhibits strong negative skewness (fat left tails).

3. Model

The model used as the basis of our simulation is the general affine jump diffusion model of Duffie, Pan, and Singleton (2000). It is a parsimonious model which embeds five affine jump diffusion models: (i) a stochastic volatility model with no jumps (SV); (ii) a stochastic volatility model with price jumps only (SVJ-Y); (iii) a stochastic volatility model with volatility jumps only (SVJ-V); (iv) a stochastic volatility model with simultaneous but uncorrelated price and volatility jumps (SVJ-Y-V); (v) a stochastic volatility model with simultaneous

and correlated price and volatility jumps (SVJJ).

3.1. Model Specification

Suppose that S is the price process of a security that pays dividends at a constant proportional rate $\bar{\zeta}$, and $Y = \ln(S)$. The state process is $X = (Y, V)^T$, where V is the variance process with a long term variance equal to $\bar{v}$. Under the risk-neutral measure Q,

$$d\begin{pmatrix} Y_t \\ V_t \end{pmatrix} = \begin{pmatrix} r - \bar{\zeta} - \bar{\lambda}\bar{\mu} - \frac{1}{2}V_t \\ \kappa_v(\bar{v} - V_t) \end{pmatrix} dt + \sqrt{V_t}\begin{pmatrix} 1 & 0 \\ \bar{\rho}\sigma_v & \sqrt{1-\bar{\rho}^2}\sigma_v \end{pmatrix} dW_t^Q + dZ_t \tag{1}$$

where r is the interest rate, W^Q is a standard Brownian motion under Q in $\mathbb{R}^2$. Z is a pure jump process in $\mathbb{R}^2$ with a constant mean jump-arrival rate $\bar{\lambda}$ whose bivariate jump-size distribution has the transform θ through which a flexible range of distributions of jumps can be explored. The risk-neutral restriction is satisfied if and only if the risk-neutral drift $\bar{\mu} = \theta(1,0) - 1$. κ_v is the mean-revertion rate of the variance process, σ_v denotes the volatility of the variance process, $\bar{\rho}$ is the correlation between the two standard Brownian motions.

The bivariate jump transform function θ is defined by:

$$\theta(c_1, c_2) = \bar{\lambda}^{-1}(\lambda^y\theta^y(c_1) + \lambda^v\theta^v(c_2) + \lambda^c\theta^c(c_1, c_2)) \tag{2}$$

where $\bar{\lambda} = \lambda^y + \lambda^v + \lambda^c$, with

$$\theta^y(c) = \exp\left(\mu_y c + \frac{1}{2}\sigma_y^2 c^2\right) \tag{3}$$

$$\theta^v(c) = \frac{1}{1 - \mu_v c} \tag{4}$$

$$\theta^c(c_1, c_2) = \frac{\exp\left(\mu_{c,y}c_1 + \frac{1}{2}\sigma_{c,y}^2 c_1^2\right)}{1 - \mu_{c,v}c_2 - \rho_J\mu_{c,v}c_1}. \tag{5}$$

Corresponding to Equations (3) to (5), respectively, three types of jumps are incorporated

in the above transform function:

(1) jumps in price Y, with arrival intensity λ^y, and the jump size is normally distributed with mean μ_y and variance σ_y^2.

(2) jumps in variance V, with arrival intensity λ^v, and the jump size is exponentially distributed with mean μ_v.

(3) simultaneous correlated jumps in both price and variance, with arrival intensity λ^c. The jump size of the variance, z_v, is exponentially distributed with mean $\mu_{c,v}$. Given z_v, the jump size of the price is normally distributed with mean $(\mu_{c,y} + \rho_J z_v)$ and variance $\sigma_{c,y}^2$, where ρ_J is the correlation between the price jump size and the variance jump size.

By imposing certain parameter restrictions on the model, five different types of stochastic volatility models are selected:

(1) **SV** model: Stochastic volatility model without jumps, obtained by letting $\bar{\lambda} = 0$.

(2) **SVJ-Y** model: Stochastic volatility model with price jumps only, obtained by letting $\lambda^y > 0$, and $\lambda^v = \lambda^c = 0$.

(3) **SVJ-V** model: Stochastic volatility model with variance jumps only, obtained by letting $\lambda^v > 0$, and $\lambda^y = \lambda^c = 0$. This is a special case where variance jumps have no impact on the price dynamics.

(4) **SVJ-Y-V** model: Stochastic volatility model with simultaneous but uncorrelated price and variance jumps, obtained by letting $\lambda^y = \lambda^v > 0$, and $\lambda^c = 0$.

(5) **SVJJ** model: Stochastic volatility model with simultaneous and correlated price and variance jumps, obtained by letting $\lambda^c > 0$, and $\lambda^y = \lambda^v = 0$.

3.2. Pricing

Under the transform, the price of a European call option is given by (Duffie et al., 2000)

$$C(K,\tau) = G_{1,-1}(-\ln K; Y_t, V_t, \tau) - KG_{0,-1}(-\ln K; Y_t, V_t, \tau) \tag{6}$$

where

$$G_{a,b}(-\ln K; Y_t, V_t, \tau) = \frac{\psi(a, Y_t, V_t, t, T)}{2} - \frac{1}{\pi}\int_0^\infty \frac{\mathrm{Im}\left[\psi(a + i\nu b, Y_t, V_t, t, T)e^{-i\nu \ln K}\right]}{\nu} d\nu$$

where $\mathrm{Im}(\cdot)$ denotes the imaginary part of a complex number. The transform ψ of log-price state variable Y_T takes the form of $\psi(u, Y_t, V_t, t, T) = \exp(\bar{\alpha}(\tau, u) + uY_t + \bar{\beta}(\tau, u)V_t)$. By letting $b = \sigma_v\bar{\rho}u - \kappa_v$, $a = u(1-u)$, and $\gamma = \sqrt{b^2 + a\sigma_v^2}$, we have $\bar{\beta}(\tau, u) = -\frac{a(1-e^{-\gamma\tau})}{2\gamma-(\gamma+b)(1-e^{-\gamma\tau})}$, and $\bar{\alpha}(\tau, u) = \alpha_0(\tau, u) - \bar{\lambda}\tau(1 + \bar{\mu}u) + \bar{\lambda}\int_0^\tau \theta(u, \bar{\beta}(s, u))ds$ with $\alpha_0(\tau, u) = -r\tau + (r - \bar{\zeta})u\tau - \kappa_v\bar{v}\left(\frac{\gamma+b}{\sigma_v^2}\tau + \frac{2}{\sigma_v^2}\ln\left[1 - \frac{\gamma+b}{2\gamma}(1 - e^{-\gamma\tau})\right]\right)$. The term $\int_0^\tau \theta(u, \bar{\beta}(s, u))ds$ depends on the specification of bivariate jump transform function θ.

Based on the specification of the bivariate jump transform θ given by Equation (2)-(5), we have the following specification for the integral of θ:

$$\int_0^\tau \theta(u, \bar{\beta}(s, u))ds = \bar{\lambda}^{-1}(\lambda^y f^y(u, \tau) + \lambda^v f^v(u, \tau) + \lambda^c f^c(u, \tau))$$

where

$$\begin{aligned}
f^y(u, \tau) &= \tau \exp\left(\mu_y u + \frac{1}{2}\sigma_y^2 u^2\right) \\
f^v(u, \tau) &= \frac{\gamma - b}{\gamma - b + \mu_v a}\tau - \frac{2\mu_v a}{\gamma^2 - (b - \mu_v a)^2}\ln\left(1 - \frac{(\gamma + b) - \mu_v a}{2\gamma}(1 - e^{-\gamma\tau})\right) \\
f^c(u, \tau) &= \exp\left(\mu_{c,y}u + \sigma_{c,y}^2\frac{u^2}{2}\right)d
\end{aligned}$$

where $a = u(1-u)$, $b = \sigma_v\bar{\rho}u - \kappa_v$, $c = 1 - \rho_J\mu_{c,v}u$, and

$$d = \frac{\gamma - b}{(\gamma - b)c + \mu_{c,v}a}\tau - \frac{2\mu_{c,v}a}{(\gamma c)^2 - (bc - \mu_{c,v}a)^2}\ln\left[1 - \frac{(\gamma + b)c - \mu_{c,v}a}{2\gamma c}(1 - e^{-\gamma\tau})\right]$$

3.3. Closed-Form RND Function

Breeden and Litzenberger (1978) show that, given a continumm of call option prices $C(K,\tau)$ with strike price K and time-to-maturity τ, and if call option prices satisfy the non-arbitrage conditions, then there exists a risk-neutral probability, the relations between the call option price and the risk-neutral probability's cumulative distribution function (cdf) F^* and risk-neutral density function f^* evaluated at the termianl price S_T are given by $\frac{\partial C(K,\tau)}{\partial K}\big|_{K=S_T} = e^{-r\tau}(F^*(K)-1)$ and $\frac{\partial^2 C(K,\tau)}{\partial K^2}\big|_{K=S_T} = e^{-r\tau}f^*(K)$.

Analogous to the Black-Scholes formula, and by applying the relation between the call option price function (Equation (6)) and the risk-neutral distribution, the following is obtained

$$\frac{\partial C(K,\tau)}{\partial K}\big|_{K=S_T} = e^{-r\tau}(F^*-1) = -G_{0,-1}(-\ln S_T; Y_t, V_t, \tau)$$

Rearranging the above equation, we obtain the cumulative distribution function evaluated at $K = S_T$

$$F^*(S_T) = 1 - e^{r\tau}G_{0,-1}(-\ln S_T; Y_t, V_t, \tau) \tag{7}$$

F^* represents the probability of $S_T < K$ under the risk-neutral measure Q. The model-derived risk-neutral density is therefore obtained by the first-order derivative of F^* with respect to K evaluated at S_T:

$$f^*(S_T) = \frac{\partial F^*}{\partial K}\big|_{K=S_T} = \frac{e^{r\tau}}{\pi S_T}\int_0^\infty \mathrm{Im}\big[\psi(-i\nu, Y_t, V_t, t, T)e^{i\nu \ln S_T} \times i\big]d\nu \tag{8}$$

4. Data

The data for model calibration and option price fitting are end-of-month options written on 1/100 Dow Jones Industrial Average index (Ticker symbol: 'DJX') over the period from March 2007 to February 2009, and are obtained from the Chicago Board Options Exchange

(CBOE). Several filters are applied to construct the option data sample:

(1) Firstly, options with zero bid quotes are excluded;

(2) Options with less than 7-day time to maturity are excluded since these options are generally illiquid and are affected by market microstructure factors.

(3) In-the-money (ITM) options are excluded. This is due to that ITM options are typically overpriced, and less liquid than at-the-money (ATM) and OTM options.

(4) Options that violate basic no-arbitrage conditions are excluded.

In addition to the option filters, robust forward prices are used; details are referred to (Lu, 2019, Appendix). On each trading day, out-of-money (OTM) options including both call and put options with three target time-to-maturities (3 weeks, 3 months and 6 months) are selected from the cleaned option data sample.[1]

Daily constant maturity treasury (CMT) rates are used as risk-free rates and are obtained from the Board of Governors of the Federal Reserve System. Various maturities, ranging from one-month to thirty-year rates, are available. Interest rates with intermedia maturities are linearly interpolated, and interest rates with maturities that are beyond available ranges are estimated by a natural cubic spline extrapolation.

Mid bid-ask prices are used as option prices to eliminate the bounce effect (Bakshi, Cao, and Chen, 2000), and the spread effect (Figlewski, 1997). Option's time to maturity is calculated by the number of calendar days remaining to maturity less one (Dumas, Fleming, and Whaley, 1998) for AM-expiration options.

[1]Following the convention for time calculation, time to maturities are expressed in calendar days. 3 weeks, 3 months, and 6 months correspond to 21, 91 and 182 calendar days, respectively.

5. Analysis of RND Methods

5.1. Fitting Market Prices of Options

The performance analysed in this section measures how well each model and estimation method fits the market option prices. The true option data are used for the analysis of the fitting performance of market prices of options.

The procedure of fitting option prices is as follows. On the one hand, for all the five stochastic volatility models and four estimation methods (LN2, HPGC, GEV, PCA), the parameters are estimated by minimizing the sum of squared pricing errors (SSE) between the option's market price $C_t(K_i)$ and the fitted option price $\hat{C}_t(K_i)$ for the ith strike price K_i at time t

$$\min\{SSE(t)\} = \min\left\{\sum_{i=1}^{N}\left(C_t(K_i) - \hat{C}_t(K_i)\right)^2\right\} \tag{9}$$

On the other hand, the objective function of the GB2 method includes not only the sum of squared pricing errors, but also the martingale condition which ensures that the mean of the RND equal the forward price. With regard to the CS method, the objective function contains two parts: the first part is the vega-weighted squared distance between estimated and observed implied volatilities in the delta space which controls the goodness-of-fit, and the second part is the integrated squared second derivative of the implied volatility which controls the smoothness of the RND, multiplied by a parameter controlling the tradeoff between the two parts, and similar to Bliss and Panigirtzoglou (2004), the smoothing parameter is set to 0.99. Subject to the QP method, the implied volatility curve is first fitted to a quadratic polynomial function of the strike price, the fitted option prices are then obtained by plugging the fitted implied volatility curve into the Black-Scholes formula. For the SRM method, by minimizing the RND smoothness function with respect to no-arbitrage and bid-ask constraints, option prices are obtained by a singular value decomposition. The $SSE(t)$ for QP and SRM is then obtained by using Equation (9).

The fitting performance is measured in terms of the root mean square error (RMSE) with

the following specification

$$RMSE(t) = \sqrt{\frac{SSE(t)}{N}}$$

The RMSE represents the average pricing error in U.S. cents per option. For each of the three target time-to-maturities (3 weeks, 3 months and 6 months), each affine jump diffusion model and each estimation method, the RMSE is taken over the period from March 2007 to February 2009.

To quantify and visualise the the fitting error across different moneyness levels, we define the fitting bias of an option as the deviation of the fitted price with respect to the market price of the option

$$\text{Fitting Bias} = \text{Market Price} - \text{Fitted Price}$$

Since moneyness levels vary from day to day, the pricing biases for different moneyness levels on each trading day are obtained by fitting a cubic spline to the pricing bias as a function of moneyness for each model, each estimation method and each time-to-maturity.

5.2. Monte Carlo Simulation

To compare the performance of eight estimation methods presented in Table 1, a Monte Carlo simulation is carried out. The procedure of the Monte Carlo analysis is as follows: Firstly, generating a set of artificial option data by simulating the paths of affine jump-diffusion models; Secondly, extracting RNDs from the artificial option data by RND methods in Table 1, and obtaining the true RNDs via the affine jump-diffusion models analytically by using Equation (7) and (8); Thirdly, RND estimates are then compared to the true RNDs by a goodness-of-fit test.

5.2.1. Artificial Option Data and Simulation Procedure

The artificial option data are generated through the Monte Carlo simulation by the affine jump diffusion models: the SV, SVJ-Y, SVJ-V, SVJ-Y-V, and SVJJ models.

In order to generate artificial option data, the above five stochastic volatility models are calibrated to the option data sample. The reason for model calibration is to get meaningful parameter estimates in the context of financial markets, and to simulate market conditions as close as possible. Fitted model parameters for the data-generating process are reported in Table 2. The average one-month constant maturity treasury (CMT) rates during the sample period are used as the risk-free rate r_f.

[Insert Table 2 around here]

Taking the SV model and the LN2 method as an example, the Monte Carlo analysis is performed as follows. By using the fitted SV model parameter estimates, two-year artificial index levels and its corresponding instantaneous variance levels are generated.[2] The DJIA index and instantaneous variance levels at the end of the two-year period are taken as the current index price S_t and the current instantaneous variance level V_t. Replacing the initial index level S_0 with S_t, the initial instantaneous variance level V_0 with V_t, and keeping the rest of model parameter estimates unchanged, a set of prices of call options with strike price ranging from $0.8 \times S_t$ to $1.2 \times S_t$ at 0.01 point ($1) interval ($\Delta K = \$1$)[3] with 3-week time-to-maturity is generated by the SV model using Equation (6). Price noises are added to the generated call option prices in order to simulate market frictions such as the bid-ask spread. The RND estimate is extracted from noised call option prices subject to the LN2 method. The true RND is obtained by using Equation (8) with the SV model parameters. This procedure is repeated 1000 times to obtain 1000 sets of call option prices; subsequently 1000 RND estimates subject to the LN2 method and 1000 true RNDs are obtained. Each RND estimate is then compared to its corresponding true RND by a goodness-of-fit test in order to quantify the estimation performance of the LN2 method.

[2]Exact simulation technique of Broadie and Kaya (2006) is applied to the simulation of paths of affine jump diffusion models.

[3]This simulates the DJX options market where strike prices are set to bracket the index level in minimum increments of 1 point ($100). In other words, the strike prices of DJX options are at 0.01 point ($1) interval. Details refer to the DJX options product specifications on the CBOE website.

The above simulation is repeated for each of the estimation methods in Table 1, each affine jump diffusion model (SV, SVJ-Y, SVJ-V, SVJ-Y-V, SVJJ), and each time to maturity (3 weeks, 3 months, and 6 months). Note that for each round of simulation, RNDs estimated by the estimation methods are extracted from the same set of model-generated artificial option data. In other words, each model generates 1000 sets of artificial option data for each time-to-maturity. Therefore, there are 15 panels of 1000 sets of artificial option data generated in total.

5.2.2. Noise Specification

To simulate the market frictions under realistic conditions, this paper adopts the method introduced by Bondarenko (2003a) to simulate the bid-ask spread and add noises to the generated artificial option data. The basic idea of the method is to set the bid-ask spread for options at each strike price depending on the price of the option, the size of the bid-ask spread is kept consistent with the exchange rules on the maximum bid-ask differentials. The price noise is then drawn uniformly on the interval from minus half to half of the size of the simulated bid-ask spread.

Assume a trader observes bid and ask quotes (q_K^b, q_K^a) for call options with strike price K. The trader uses the mid-point quote $C(K) = 0.5(q_K^b + q_K^a)$ as the approximated call option price. The price noise ε_K for call option struck at K is assumed to be uniformly distributed on the interval $[-0.5s_k, 0.5s_K]$, where the bid-ask spread $s_K = q_K^a - q_K^b$. The bid-ask spread s_K is proportional to the maximum bid-ask differentials allowed by the exchange trading rule. The CBOE rule on maximum bid-ask differentials changes over the years. The rule used here follows that in Bondarenko (2003a). The rule states that the maximum bid-ask differentials are: $\frac{1}{4}$ for options with bid quote q^b below \$2, $\frac{3}{8}$ for bid quotes between \$2 and \$5, $\frac{1}{2}$ for bid quotes \$5 and %10, $\frac{3}{4}$ for bid quotes between \$10 and %20, and 1 for bid quotes above \$20. According to this rule, the function for maximum bid-ask differentials $M(q)$ can

be constructed in the following way:

$$M(0) = \frac{1}{8}, M(2) = \frac{1}{4}, M(5) = \frac{3}{8}, M(10) = \frac{1}{2}, M(20) = \frac{3}{4}, M(q) = 1, q \geq 50$$

$M(q)$ is linearly interpolated for quotes $q \in [0, 50]$. In practice, since out-of-money (OTM) options are more liquid than in-the-money (ITM) options, OTM options are more accurate than ITM options. Consequently, the trader uses the put-call parity to convert ITM call option prices to OTM put option prices. Therefore, the simulated bid-ask spread is the minimum of the spreads for call $C(K)$ and put $P(K) = C(K) - S + K$:

$$s_K = c \times \min(M(C(K)), M(C(K) - S + K))$$

where c is a constant which controls the level of noise, ranging from 0 to 1. In this paper, c is set equal to 1, meaning that the simulated bid-ask spread equal the maximum bid-ask differentials allowed by the exchange regulation.[4] Figure 1 shows an example of the OTM option prices, and simulated bid-ask spreads and price noises. This method is consistent with the empirical findings in the market bid-ask spread. For example, Dumas et al. (1998) find that the behaviour of bid-ask spread is consistent with the maximum bid-ask differentials allowed by the CBOE for S&P 500 index options from 1988 to 1993.

[Insert Figure 1 around here]

The advantage of this method is that the absolute (relative) noise is smaller (larger) for far-from-the-money options, and simulated option prices are ensured to be nonnegative (Bondarenko, 2003a).

[4] Bondarenko (2003a) reports that different values of constant c have negligible impact on the evaluation of performance of methods for option-implied densities.

5.2.3. Goodness-of-Fit Test

To illustrate the simulation, two examples are given. Firstly, RNDs of the affine jump-diffusion models are depicted in Figure 2; these RNDs are generated by affine jump-diffusion models by plugging the parameter estimates presented in Table 2 into Equation (8). Secondly, RND estimates from a single round of Monte Carlo simulation are depicted in Figure 3; the true RND (solid line) is generated by the SV model with parameter estimates from Table 2 and the simulated underlying index level $S_t = 101.22$, instantaneous variance level $V_t = 0.0107$, and strike price $K \in [80, 121]$; the estimated RNDs (dashed lines) are extracted by eight estimation methods from the same set of artificial option data generated by the SV model perturbed by the noise perturbation process. Figure 2 shows that models with (either price or volatility or both) jumps produce fatter left tails than those produced by the model without jumps (SV model); the SVJJ model produces the fattest left tail. RNDs of the SVJ-V and SVJJ models are more leptokurtic than the RND produced by the SV model; none of the RNDs generated seem to be near a normal distribution. Figure 3 shows that for most methods, the estimated RNDs differ from the true RND the most in the tail areas of the RND, this is consistent with observations in Jackwerth (1999); Lai (2014). However, it is difficult to decide which method produces the RND estimate with the most precision from either reading the figures or computing error statistics, since the level of dispersion differs at different strike ranges. Therefore, it requires a statistical test to quantify the performance of each method in terms of precision of density estimates.

[Insert Figure 2 around here]

[Insert Figure 3 around here]

The Kolmogorov-Smirnov two-sample test is employed to compare the estimation performance of the RND methods. The advantage of the Kolmogorov-Smirnov test is its consistency (Kendall and Stuart, 1979; Jackwerth, 2004). The test is a nonparametric method for evaluating density estimates. It tests whether two sample distributions come from the same

distribution function. Assuming two samples drawn from cumulative distribution functions F_1 and F_2, and these samples have empirical distribution functions $\hat{F}_1$ and $\hat{F}_2$, the null hypothesis of the Kolmogorov-Smirnov two-sample test is then $H_0 : F_1 = F_2$. The test statistic of the test is the maximum difference between the two empirical cumulative distribution functions. Analogously, we are testing whether the estimated risk-neutral cumulative distribution function $\hat{F}^*$ is the same as model-derived true risk-neutral cumulative distribution function F^*:

$$H_0 : \hat{F}^*(S_T) = F^*(S_T) \tag{10}$$

The true F^* is computed by using Equation (7); and the estimated $\hat{F}^*$ can be computed either analytically or numerically depending on the estimation method used.

5.2.4. Sensitivity to the Discreteness of Option Prices

Table 3 reports the average number of option strikes per cross section in the artificial options data generated by different affine jump diffusions. At 0.01 point ($1) interval, the average number of option strikes per cross section ranges from 47 to 54. However, this average number of option strikes per cross section is higher than the actual market data reported in the literature. For example, Liu et al. (2007) reports that average number of option strikes of FTSE 100 index options is 37 per month from 1993 to 2003. For stock options, the number of option strikes per cross section can sometimes be under 15 or less. Therefore, the performance of RND methods when performing estimations on a sparse data with a low number of option strikes is also examined.

[Insert Table 3 around here]

The procedure is as follows. From the generated artificial options data where option strike prices are at 0.01 point ($1) interval, option contracts are selected on a sparser strike price grid, and the new strike price grid is at 0.05 points ($5). After the selection, the

average number of option strikes per cross section at 0.05 points reduces to approximately 11 (Table 3), and is as low as 3 option strikes per cross section. RND methods are then used to back out the entire RND, and the estimated RND is compared to the true RND by the goodness-of-fit test.

6. Results

6.1. Fitting Bias Across Time to Maturity

Table 4 presents the fitting performance in terms of the average RMSE across the sample period for OTM calls, OTM puts and all OTM options, respectively. Panel A shows that SVJ-Y-V and SVJJ provide the best fitting performance for 3-week and 3-month time-to-maturities, whereas they do not have the best overall fitting performance for options with 6-month time-to-maturity, however, they do provide best fittings for OTM put options. The SV model has the worst fitting performance in all instances. The results are consistent with the equity price dynamics and option pricing literature (e.g. Broadie et al., 2007), and reinforce that both price and volatility jumps are important pricing components, and have to be taken into account. Panel B shows that: CS provides the best fitting performance whereas HPGC performs the worst. The performance of PCA is very close to CS for the shortest maturity, however, the performance of PCA becomes worser than CS for longer maturities. GB2 performs worse than GEV which belongs to the same method category. GEV and QP have roughly the same fitting performance, and they outperform SRM. LN2 is the second to last in terms of fitting option prices. Besides, two clear patterns that can be observed from Panel B are, despite of the estimation methods and time-to-maturity: (1) the fitting errors increase with the time-to-maturity; (2) the fitting errors for OTM calls are larger than those for OTM puts.

[Insert Table 4 around here]

6.2. Fitting Bias across Moneyness

The average of the cubic splines over the sample period are depicted in Figure 4. Fitting biases are shown only for moneyness levels ranging from 0.8 to 1.14.[5]

[Insert Figure 4 around here]

Figure 4 shows that among stochastic volatility models, there are trivial differences in the fitting performance for near-the-money options for all three time-to-maturities, while relatively large differences occur for away-from-the-money options. For example, for 3-week (21-day) time-to maturity, differences are observed for OTM call options with moneyness larger than 1.07, SVJJ and SVJ-V have smaller fitting biases compared to other models. For 3-month (91-day) time-to-maturity, differences occur mainly for OTM put options, and the SV model performs relatively poorer than other models. For 6-month (182-day) time-to-maturity, fitting differences are observable for both far-from-the-money OTM call and put options.

Concerning fitting bias of the estimation methods, SRM performs the worst while the LN2 yields the best fitting performance for OTM call options for the shortest time-to-maturity. Moving to 3-month time-to-maturity, it is observed that while there are no large differences among methods except for the HPGC; the HPGC provides the worst fitting performance for options with moneyness smaller than approximately 1.12, and yields the best the performance for options with moneyness larger than 1.12. The magnitudes of differences in fitting bias are much larger for the longest time-to-maturity; HPGC is ranked the last in terms of fitting bias for away-from-the-money options, while the SRM seems to outperform other methods for options with moneyness levels up to 1.13.

[5]The moneyness range is selected according to the average moneyness levels across the sample period. There are very few data points outside the selected moneyness range to obtain meaningful average pricing biases. Moneyness is defined as K/S.

6.3. Estimation Performance of RND Methods

Table 5 presents the mean and the standard deviation of p-values of the Kolmogorov-Smirnov test; the standard deviation of p-values is computed from a set of 1000 RND estimates; the rejection rate is the percentage of density estimates rejected at 5% significance level, and is calculated by dividing the number of p-values smaller than 0.05 by the total number of p-values (which is 1000). From Table 5, two patterns are identified: Firstly, the rejection rate is higher for RND estimates at the shortest time-to-maturity (3 weeks) than those at longer time-to-maturities, regardless of models and estimation methods; the only exception is the HPGC and GEV under the SV model, and HPGC under the SVJ-V model, where the rejection rate increases with the time-to-maturity; for all three nonparametric methods this pattern hold without exception. Secondly, the rejection rate increases as the underlying process becomes complicated (the inclusion of price and volatility jumps).

[Insert Table 5 around here]

Concerning the rejection rate, the largest dispersion in the estimation performance occurs at the shortest time-to-maturity (3 weeks): among four parametric methods, the HPGC method is the best performer while LN2 performs the worst, especially under the SVJJ process; GEV performs well but its performance dramaticaly worsens when correlated price and volatility jumps are introduced into the underlying process; GB2's performance is identical to GEV, but is better under the SVJJ process. Among four nonparametric methods, PCA provides the most accurate RND estimates, while QP performs the worst under most models except the SVJ-V model. When they are compared together, PCA has the best performance and consistency, this is confirmed by its lowest variation (measured by standard deviation) in p-values. Note that the performance of CS is close to that of PCA with only a few exceptions such as under the SV and SVJ-V processes, but CS offers a lower average and a higher standard deviation of the p-value than PCA. LN2 is ranked the last; parametric methods HPGC, GB2 and GEV consistently outperforms nonparametric QP, and they also

outperforms nonparametric SRM except for the SVJJ process. Moving to longer time-to-maturities (3 and 6 months), the differences in the estimation performance diminishes. For most methods, the rejection rate is low and near zero. Note that except for the HPGC whose performance worsens with the increasing time-to-maturity, the performance of other methods remain almost unchanged for 91 and 182 days time-to-maturities. It should be noted that, despite the underlying process, while the rejection rate for SRM is around 2 to 4%, its average p-value stands at a high level between 0.94 to 0.98, implying that the rejection rate is largely attributed to a small number of outliers, the interquartile range of the p-values for SRM is expected to be narrow.

Figures 5-9 visualize the distribution of these p-values; they show the box plot of Kolmogorov-Smirnov p-values; the red line in each box represents the median p-value; each box covers the interquartile range of the Kolmogorov-Smirnov p-values, the upper and lower edges of the box correspond to the 25th and 75th percentiles of the p-value sample; the whiskers are marked at 1.5 times the interquartile range; outliers are plotted individually by using red "+" symbols. These figures reinforce our observations from the rejection rate.

[Insert Figure 5 around here]

[Insert Figure 6 around here]

[Insert Figure 7 around here]

[Insert Figure 8 around here]

[Insert Figure 9 around here]

6.4. Results of Sensitivity to the Discreteness of Option Prices

Table 6 reports both the magnitude and direction of the change in the Kolmogorov-Smirnov p-value when the option strikes become sparser (ΔK changes from \$1 to \$5). Changes in the average p-value ($\Delta\bar{p}$) is calculated as: $\bar{p}_{\Delta K=5} - \bar{p}_{\Delta K=1}$, and changes in the rejection rate (ΔRejection) is calculated as: $\text{Rejection}_{\Delta K=5} - \text{Rejection}_{\Delta K=1}$. A negative

$\Delta\bar{p}$ or a positive ΔRejection indicates a worse performance, and a positive $\Delta\bar{p}$ or a negative ΔRejection indicates a better performance, when performing estimations on sparser options data with fewer number of options. For most methods except the LN2, QP and CS, a sparse strike price grid and a low number of strikes per cross section lower the average Kolmogorov-Smirnov p-values, whereas the average p-value for LN2 increases as data become sparse; both directions of change in the average p-value are possible for QP and CS. Concerning the impact on the rejection rate, PCA is the most insensitive to the discreteness of option prices, while sparseness has the largest impact on the LN2. Note that when the underlying asset price incorporates double jumps, a sparse data would lower the performance of almost all the RND methods examined, especially for the shortest maturity, and the magnitude is relative large, except for the LN2 whose performance changes adversely. For GEV and QP, both directions of change in the performance is possible.

[Insert Table 6 around here]

In the supplementary data, Table 7 reports the performance of RND methods when performing estimations on options data with strike price at 0.05 points interval and an average of 11 option strikes per cross section. Figures 10-14 present the boxplots of the Kolmogorov-Smirnov p-value. The relative performance of RND methods doesn't change compared to the case of a denser strike price grid.

7. Conclusion

This paper compares several estimation methods for extracting risk-neutral densities (RND) from option prices via a pseudo-price based Monte Carlo simulation. It is motivated by the paucity of research in the comparison of widely-used and recently-developed methods for extracting RNDs from option prices. Methods compared in the paper are: mixture of two lognormals (LN2) of Ritchey (1990), hermite polynomial with Gram-Charlier expansion (HPGC) of Jondeau and Rockinger (2001), generalized beta distribution of the second

kind (GB2) of Bookstaber and MacDonald (1987), generalized extreme value distribution (GEV) of Markose and Alentorn (2011), curve-fitting with quadratic polynomial (QP) of Shimko (1993), curve-fitting with cubic smoothing spline (CS) of Bliss and Panigirtzoglou (2004), positive convolution approximation (PCA) of Bondarenko (2000, 2003a) and spectral recovery method (SRM) of Monnier (2013).

It is shown that the kernel method of PCA consistently yields the most accurate RND estimates and is insensitive to the discreteness of option prices, whereas the LN2 method performs the worst. HPGC is the best performer among parametric methods; both HPGC, GB2 and GEV in the parametric domain outperforms the QP in the nonparametric domain. While the SRM has a higher rejection rate than HPGC, GB2 and GEV, SRM has a higher mean Kolmogorov-Smirnov p-value and its interquartile range is narrower than those for HPGC, GB2 and GEV, implying that the higher rejection rate of SRM may be attributed to minor outliers. Besides, RND methods are less likely to produce accurate RND estimates when the underlying process incorporates jumps and when data are sparse, especially for short time-to-maturities, though sensitivity to the discreteness of the data differs across different methods; In addition, through the comparison of the fitting performance of affine jump diffusion models, we show that models with both price and volatility jumps outperform others, reinforcing the findings in the equity price dynamics and option pricing literature that both price and volatility jumps are important components for option pricing.

Our research has important implications, particularly, for decision-makers at business firms and policymakers at central banks, since risk-neutral densities are important indicators for market sentiment and expectations, and they are useful in the pricing of complex derivatives. It is suggested that the shape of risk-neutral densities vary over time, it may be insufficient to assume a single parametric form of the distribution. Our results suggest that nonparametric methods such as PCA are capable of providing the most accurate yet consistent RND estimates.

References

Abadir, K., Rockinger, M., 2003. Density functionals, with an option-pricing application. Econometric Theory 19, 778–811.

Abken, P., Madan, D., Ramamurtie, S., 1996. Estimation of risk-neutral and statistical densities by hermite polynomial approximation, working paper, Federal Reserve Bank of Atlanta.

Aït-Sahalia, Y., Lo, A., 1998. Nonparametric estimation of state-price densities implicit in financial asset prices. Journal of Finance 53, 499–547.

Anagnou, I., Bedendo, M., Hodges, S., Tompkins, R., 2002. The relation between implied and realized probability density functions, working paper, University of Warwick.

Andersen, A., Wagener, T., 2002. Extracting risk neutral probability densities by fitting implied volatility smiles: Some methodological points and an application to the 3m euribor futures option prices, working paper, European Central Bank.

Aparicio, S., Hodges, S., 1998. Implied risk-neutral distributions: A comparison of estimation methods, working paper, University of Warwick.

Bahra, B., 2007. Implied risk-neutral probability density functions from option prices: a central bank perspective. In: Knight, J., Satchell, S. (eds.), *Forecasting Volatility in the Financial Markets: A volume in Quantitative Finance*, Butterworth-Heinemann, pp. 201–226.

Bakshi, G., Cao, C., Chen, Z., 2000. Pricing and hedging long-term options. Journal of Econometrics 94, 277–318.

Bali, T., Murray, S., 2013. Does risk-neutral skewness predict the cross-section of equity option portfolio returns? Journal of Financial and Quantitative Analysis 48, 1145–1171.

Birru, J., Figlewski, S., 2012. Anatomy of a meltdown: The risk neutral density for the s&p 500 in the fall of 2008. Journal of Financial Markets 15, 151–180.

Bliss, R., Panigirtzoglou, N., 2002. Testing the stability of implied probability density functions. Journal of Banking and Finance 26, 381–422.

Bliss, R., Panigirtzoglou, N., 2004. Option-implied risk aversion estimates. Journal of Finance 59, 407–446.

Bondarenko, O., 2000. Recovering risk-neutral densities: A new nonparametric approach, working paper, University of Illinois at Chicago.

Bondarenko, O., 2003a. Estimation of risk-neutral densities using positive convolution approximation. Journal of Econometrics 116, 85–112.

Bondarenko, O., 2003b. Statistical arbitrage and securities prices. Review of Financial Studies 16, 875–919.

Bookstaber, R., MacDonald, J., 1987. A general distribution for describing security price returns. Journal of Business 60, 401–424.

Breeden, D., Litzenberger, R., 1978. Prices of state-contingent claims implicit in option prices. Journal of Business 51, 621–651.

Broadie, M., Chernov, M., Johannes, M., 2007. Model specification and risk premia: Evidence from futures options. Journal of Finance LXII, 1453–1490.

Broadie, M., Kaya, Ö., 2006. Exact simulation of stochastic volatility and other affine jump diffusion processes. Operations Research 54, 217–231.

Bu, R., Hadri, K., 2007. Estimating option implied risk-neutral densities using spline and hypergeometric functions. Econometrics Journal 10, 216–244.

Derman, E., Kani, I., 1994. Riding on a smile. Risk 7, 32–39.

Duffie, D., Pan, J., Singleton, K., 2000. Transform analysis and asset pricing for affine jump-diffusions. Econometrica 68, 1343–1376.

Dumas, B., Fleming, J., Whaley, R., 1998. Implied volatility functions: Empirical tests. Journal of Finance 53, 2059–2106.

Eriksson, A., Ghysels, E., Wang, F., 2009. The normal inverse gaussian distribution and the pricing of derivatives. Journal of Derivatives 16, 23–37.

Figlewski, S., 1997. Forecasting volatility. Financial Markets, Institutions & Instruments 6, 1–88.

Figlewski, S., 2018. Risk neutral densities: A review. Annual Review of Financial Economics 10, 329–359.

Garcia, R., Lewis, M., Pastorello, S., Renault, E., 2011. Estimation of objective and risk-neutral distributions based on moments of integrated volatility. Journal of Econometrics 160, 22–32.

Hardle, W., Yatchew, A., 2002. Dynamic nonparametric state price density estimation using constrained least squares and the bootstrap, working paper, Humboldt University Berlin.

Ivanova, V., Gutiérrez, J., 2014. Interest rate forecasts, state price densities and risk premium from euribor options. Journal of Banking and Finance 48, 210–223.

Jackwerth, J., 1999. Option implied risk-neutral distributions and implied binomial trees: A literature review, working paper, Universität Konstanz.

Jackwerth, J., 2000. Recovering risk aversion from option prices and realized returns. Review of Financial Studies 13, 433–451.

Jackwerth, J., 2004. Option-Implied Risk-Neutral Distributions and Risk Aversion. The Research Foundation of AIMR, Charlottesville, USA.

Jondeau, E., Rockinger, M., 2001. Gram-charlier densities. Journal of Economic Dynamics and Control 25, 1457–1483.

Kendall, M., Stuart, A., 1979. The advanced theory of statistics, vol. 2. Oxford University Press, New York.

Lai, W.-N., 2014. Comparison of methods to estimate option implied risk-neutral densities. Quantitative Finance 14, 1839–1855.

Liu, X., Shackleton, M., Taylor, S., Xu, X., 2007. Closed-form transformations from risk-neutral to real-world distributions. Journal of Banking and Finance 31, 1501–1520.

Lu, S., 2019. Testing the predictive ability of corridor implied volatility under garch models. Asia-Pacific Financial Markets 26, 129–168.

Malz, A., 1997. Estimating the probability distribution of the future exchange rate from option prices. Journal of Derivatives 5, 18–36.

Markose, S., Alentorn, A., 2011. The generalized extreme value distribution, implied tail index, and option pricing. Journal of Derivatives 18, 35–60.

Monnier, J., 2013. Risk-neutral density recovery via spectral analysis. SIAM Journal on Financial Mathematics 4, 650–667.

Olijslagers, S., Petersen, A., de Vette, N., van Wijnbergen, S., 2018. What option prices tell us about the ecb's unconventional monetary policies, tinbergen Institute Discussion Paper 2018-096.

Ritchey, R., 1990. Call option valuation for discrete normal mixtures. Journal of Financial Research 13, 285–295.

Rockinger, M., Jondeau, E., 2002. Entropy densities with an application to autoregressive conditional skewness and kurtosis. Journal of Econometrics 106, 119–142.

Rosenberg, J., Engle, R., 2002. Empirical pricing kernels. Journal of Financial Economics 64, 341–372.

Ross, S., 2015. The recovery theorem. Journal of Finance 70, 615–648.

Rubinstein, M., 1994. Implied binomial trees. Journal of Finance 49, 771–818.

Santos, A., Guerra, J., 2015. Implied risk enutral densities from option prices: Hypergeometric, spline, lognormal, and edgeworth functions. Journal of Futures Markets 35, 655–678.

Sherrick, B., Irwin, S., Forster, D., 1996. An examination of option-implied s&p 500 futures price distributions. Financial Review 31, 667–695.

Shimko, D., 1993. Bounds on probability. Risk 6, 33–37.

Söderlind, P., 2000. Market expectations in the uk before and after the erm crisis. Economica 67, 1–18.

Taylor, S., 2005. Asset Price Dynamics, Volatility, and Prediction. Princeton University Press, Princeton, MA, USA.

Taylor, S., Tzeng, C.-F., Widdicks, M., 2014. Bankruptcy probabilities inferred from option prices. Journal of Derivatives 22, 8–31.

Völkert, C., 2015. The distribution of uncertainty: Evidence from the vix options market. Journal of Futures Markets 35, 597–624.

Xiu, D., 2014. Hermite polynomial based expansion of european option prices. Journal of Econometrics 179, 158–177.

Table 1: **Methods for Option-Implied Risk-Neutral Distributions**

Method	Abbreviation	Category	Author (year)
Mixture of two lognormal distributions	LN2	Parametric, Mixture	Ritchey (1990)
Hermite polynomial with Gram-Charlier expansion, restrictions imposed on the third and fourth moments	HPGC	Parametric, Expansion	Jondeau and Rockinger (2001)
Generalized beta distribution of the second kind	GB2	Parametric, Generalized distribution	Bookstaber and MacDonald (1987)
Generalized extreme value distribution	GEV	Parametric, Generalized distribution	Markose and Alentorn (2011)
Quadratic polynomial applied to implied volatilities	QP	Nonparametric, Curve fitting	Shimko (1993)
Cubic smoothing spline with Vega weighting applied to implied volatilities	CS	Nonparametric, Curve fitting	Bliss and Panigirtzoglou (2004)
Convolution of positive kernel	PCA	Nonparametric, Kernel	Bondarenko (2000, 2003a)
Spectral recovery	SRM	Nonparametric, Spectral analysis	Monnier (2013)

Notes: The table reports the estimation methods for extracting risk-neutral densities from option prices in comparison, including the description, model name and author(s) of the methods.

Table 2: **Fitted Parameter Values for General Affine Jump-Diffusions**

Model	SV	SVJ-Y	SVJ-V	SVJ-Y-V	SVJJ
S_0	123.55	123.55	123.55	123.55	123.55
r_f	0.0233	0.0233	0.0233	0.0233	0.0233
q	0	0	0	0	0
V_0	0.0495	0.0405	0.0545	0.0414	0.0326
κ_v	1.3749	4.7841	5.7032	4.8678	3.8492
σ_v	0.9000	0.4463	0.8616	0.4966	0.3829
$\bar{\rho}$	-0.3998	-0.8046	-0.6507	-0.7685	-0.8707
$\bar{v}$	0.0693	0.0220	0.0259	0.0236	0.0092
μ_y		-0.1492	-	-0.1526	-
σ_y		0.4316	-	0.4475	-
λ^y		0.1686	-	0.1528	-
μ_v			0.8999	-0.0094	-
λ^v			0.2244	0.1528	-
$\mu_{c,y}$					-0.0227
$\sigma_{c,y}$					0.1473
$\mu_{c,v}$					0.0248
ρ_J					-0.8951
λ^c					0.9452

Notes: The table reports the parameter estimates for SV, SVJ-Y, SVJ-V, SVJ-Y-V and SVJJ models from end-of-month options over the period from March 2007 and February 2009.

Table 3: **Average Number of Option Strikes Per Cross Section**

Discreteness	Generating Process				
	SV	SVJ-Y	SVJ-V	SVJ-Y-V	SVJJ
0.01 point ($\Delta K = \$1$)	53.47	46.85	52.51	52.63	48.68
0.05 points ($\Delta K = \$5$)	11.89	10.57	11.71	11.73	10.93

Notes: The tables reports the average number of options per cross section in the artificial options data. The discreteness of option prices is measured by the interval between two consecutive strike price points (ΔK) in US dollar.

Table 4: **Fitting Performance**

	$\tau = 21$			$\tau = 91$			$\tau = 182$		
	Call	Put	All	Call	Put	All	Call	Put	All
Panel A:									
SV	8.60	8.26	8.42	5.75	6.59	6.41	6.84	7.77	7.32
SVJ-Y	3.93	3.00	3.37	4.76	3.97	4.27	6.07	6.80	6.41
SVJ-V	7.06	6.38	6.66	5.69	5.30	5.48	6.80	6.88	6.75
SVJ-Y-V	3.62	2.77	3.10	4.95	3.72	4.22	7.38	6.66	6.91
SVJJ	3.99	2.92	3.34	4.67	3.47	3.94	7.41	6.71	6.96
Panel B:									
LN2	7.79	6.36	7.01	10.68	5.74	8.03	15.03	9.65	12.22
HPGC	16.20	11.89	13.48	35.68	31.97	33.22	49.29	51.58	49.85
GB2	6.82	5.44	5.95	7.00	6.38	6.76	9.06	8.26	8.75
GEV	4.31	3.44	3.80	5.70	4.91	5.32	8.73	7.13	8.04
QP	4.86	3.10	3.85	5.91	4.51	5.23	8.63	7.75	8.30
CS	3.23	2.24	2.63	2.47	1.92	2.13	2.82	2.46	2.60
PCA	3.29	2.33	2.72	6.16	3.39	4.63	9.51	5.92	7.73
SRM	6.34	4.27	5.23	8.44	4.40	6.37	13.80	4.84	10.32

Notes: The table reports the fitting performance of affine jump diffusion models and RND methods in terms of the average RMSE across the sample period for OTM calls, OTM puts and all OTM options, respectively. Fitting performance is measured by average root mean squared error for out-of-money call and put option prices in US cents.

Table 5: **Summary Statistics of p-values of the Kolmogorov-Smirnov Test ($\Delta K = \$1$)**

	$\tau = 21$			$\tau = 91$			$\tau = 182$		
	Average p-value	Standard Deviation	Rejection of H_0 (%)	Average p-value	Standard Deviation	Rejection of H_0 (%)	Average p-value	Standard Deviation	Rejection of H_0 (%)
SV process									
LN2	0.09	0.18	68.1	0.52	0.21	0.2	0.97	0.04	0.0
HPGC	0.98	0.08	0.1	0.84	0.27	1.9	0.75	0.31	4.9
GB2	0.78	0.31	2.0	0.99	0.05	0.1	0.99	0.06	0.1
GEV	0.96	0.11	0.2	0.96	0.10	0.0	0.83	0.33	4.2
QP	0.62	0.37	8.8	0.99	0.02	0.0	1.00	0.00	0.0
CS	0.99	0.03	0.0	0.98	0.09	0.2	0.93	0.19	1.2
PCA	1.00	0.00	0.0	1.00	0.00	0.0	1.00	0.00	0.0
SRM	0.95	0.21	4.4	0.98	0.15	2.1	0.97	0.17	2.8
SVJ-Y process									
LN2	0.03	0.06	82.1	0.41	0.18	0.0	0.93	0.07	0.0
HPGC	1.00	0.01	0.0	0.94	0.11	0.0	0.83	0.11	0.0
GB2	0.96	0.10	0.0	0.98	0.05	0.0	1.00	0.00	0.0
GEV	0.97	0.10	0.0	0.88	0.24	0.5	0.98	0.04	0.0
QP	0.45	0.27	4.3	0.85	0.16	0.0	1.00	0.01	0.0
CS	1.00	0.01	0.0	0.99	0.02	0.0	0.98	0.07	0.0
PCA	1.00	0.00	0.0	1.00	0.00	0.0	1.00	0.00	0.0
SRM	0.98	0.12	1.5	0.99	0.11	1.3	0.98	0.13	1.8
SVJ-V process									
LN2	0.07	0.15	71.5	0.49	0.24	1.1	0.95	0.08	0.0
HPGC	0.95	0.16	0.8	0.84	0.27	3.7	0.70	0.26	4.7
GB2	0.91	0.19	0.1	0.98	0.08	0.4	1.00	0.03	0.0
GEV	0.96	0.12	0.1	0.92	0.19	0.2	0.96	0.07	0.0
QP	0.76	0.23	0.2	0.97	0.07	0.0	1.00	0.02	0.0
CS	0.99	0.06	0.3	0.97	0.15	1.0	0.91	0.22	2.2
PCA	1.00	0.00	0.0	1.00	0.00	0.0	1.00	0.00	0.0
SRM	0.97	0.17	2.8	0.98	0.15	2.3	0.98	0.15	2.1
SVJ-Y-V process									
LN2	0.02	0.04	94.1	0.35	0.13	0.0	0.92	0.06	0.0
HPGC	0.99	0.03	0.0	0.92	0.13	0.0	0.78	0.10	0.0
GB2	0.95	0.11	0.0	0.98	0.04	0.0	1.00	0.00	0.0
GEV	0.95	0.12	0.0	0.87	0.24	1.1	0.97	0.04	0.0
QP	0.39	0.25	6.9	0.83	0.16	0.0	1.00	0.01	0.0
CS	1.00	0.01	0.0	1.00	0.02	0.0	0.97	0.07	0.0
PCA	1.00	0.00	0.0	1.00	0.00	0.0	1.00	0.00	0.0
SRM	0.97	0.17	3.0	0.98	0.14	2.0	0.98	0.14	2.0
SVJJ process									
LN2	0.02	0.04	91.4	0.35	0.14	0.2	0.92	0.06	0.0
HPGC	0.75	0.34	2.8	0.66	0.23	0.0	0.65	0.15	0.0
GB2	0.58	0.41	11.4	0.62	0.33	0.0	0.90	0.11	0.0
GEV	0.56	0.43	23.0	0.61	0.33	4.9	0.66	0.26	0.0
QP	0.40	0.32	25.9	0.79	0.18	0.0	0.99	0.02	0.0
CS	0.86	0.24	0.0	1.00	0.00	0.0	0.99	0.02	0.0
PCA	0.93	0.15	0.0	0.94	0.08	0.0	0.99	0.01	0.0
SRM	0.94	0.22	4.7	0.97	0.17	3.1	0.97	0.18	3.2

Notes: The table reports the mean and the standard deviation of p-values of the Kolmogorov-Smirnov test of the estimation performance of methods for RND. The standard deviation of p-values is computed from a set of 1000 RND estimates; the rejection rate is the percentage of density estimates rejected at 5% significance level, and is calculated by dividing the number of p-values smaller than 0.05 by the total number of p-values (which is 1000).

Table 6: **Changes in the Kolmogorov-Smirnov p-values**

Generating Processes	LN2	HPGC	GB2	GEV	QP	CS	PCA	SRM
Panel A: Changes in the Average p-value, $\Delta\bar{p}$								
$\tau = 21$								
SV	0.00	-0.05	0.01	-0.01	-0.03	-0.06	-0.02	-0.06
SVJ-Y	0.03	-0.01	-0.01	-0.00	0.09	-0.01	-0.00	-0.03
SVJ-V	0.04	-0.02	0.00	0.00	-0.07	-0.03	-0.01	-0.04
SVJ-Y-V	0.03	-0.01	-0.01	0.00	0.10	-0.01	-0.00	-0.02
SVJJ	0.05	-0.00	-0.01	0.01	0.02	-0.11	-0.10	-0.16
$\tau = 91$								
SV	0.00	0.00	0.00	0.01	-0.01	0.01	-0.00	-0.01
SVJ-Y	0.01	0.00	-0.01	0.09	0.04	0.00	-0.00	-0.01
SVJ-V	0.01	0.00	-0.00	0.03	0.01	0.02	-0.00	-0.00
SVJ-Y-V	0.01	0.00	-0.01	0.10	0.04	0.00	-0.00	-0.00
SVJJ	0.02	-0.01	-0.03	-0.12	0.00	-0.00	-0.01	-0.01
$\tau = 182$								
SV	-0.00	0.00	0.01	0.16	0.00	0.05	-0.00	-0.00
SVJ-Y	0.01	0.00	-0.00	-0.00	0.00	0.02	0.00	-0.00
SVJ-V	0.00	0.00	0.00	-0.00	0.00	0.06	-0.00	-0.00
SVJ-Y-V	0.01	0.00	-0.00	-0.00	0.00	0.02	-0.00	-0.00
SVJJ	-0.01	-0.01	-0.00	-0.54	-0.00	0.01	0.00	-0.00
Panel B: Changes in the Rejection Rate (%), ΔRejection								
$\tau = 21$								
SV	4.8	0.0	-1.7	-0.2	8.2	0.0	0.0	-0.2
SVJ-Y	-4.8	0.0	0.0	0.0	-3.5	0.0	0.0	2.0
SVJ-V	-1.9	-0.2	0.0	0.1	0.8	-0.2	0.0	-0.2
SVJ-Y-V	-4.9	0.0	0.0	0.0	-6.3	0.0	0.0	0.6
SVJJ	-9.0	1.9	3.1	-0.7	2.5	2.7	0.3	0.3
$\tau = 91$								
SV	0.0	-0.1	-0.1	0.0	0.0	-0.1	0.0	0.0
SVJ-Y	0.4	0.0	0.0	-0.5	0.0	0.0	0.0	0.5
SVJ-V	-0.1	0.0	-0.3	-0.1	0.0	-0.8	0.0	0.0
SVJ-Y-V	0.2	0.0	0.0	-1.1	0.0	0.0	0.0	-0.2
SVJJ	0.7	0.0	0.0	4.4	0.0	0.0	0.0	0.0
$\tau = 182$								
SV	0.0	-0.1	-0.1	-4.1	0.0	-0.8	0.0	0.0
SVJ-Y	0.0	0.0	0.0	0.0	0.0	0.0	0.0	0.3
SVJ-V	0.0	0.0	0.0	0.1	0.0	-1.7	0.0	0.2
SVJ-Y-V	0.0	0.0	0.0	0.0	0.0	0.0	0.0	0.0
SVJJ	0.0	0.0	0.0	0.0	0.0	0.0	0.0	0.1

Notes: The table reports both the magnitude and direction of the change in the Kolmogorov-Smirnov p-value when the option strikes become sparser (ΔK changes from \$1 to \$5). Changes in the average p-value ($\Delta\bar{p}$) is calculated as: $\bar{p}_{\Delta K=5} - \bar{p}_{\Delta K=1}$, and changes in the rejection rate (ΔRejection) is calculated as: $\text{Rejection}_{\Delta K=5} - \text{Rejection}_{\Delta K=1}$. A negative $\Delta\bar{p}$ or a positive ΔRejection indicates a worse performance, and a positive $\Delta\bar{p}$ or a negative ΔRejection indicates a better performance, when performing estimations on sparser options data with fewer number of options.

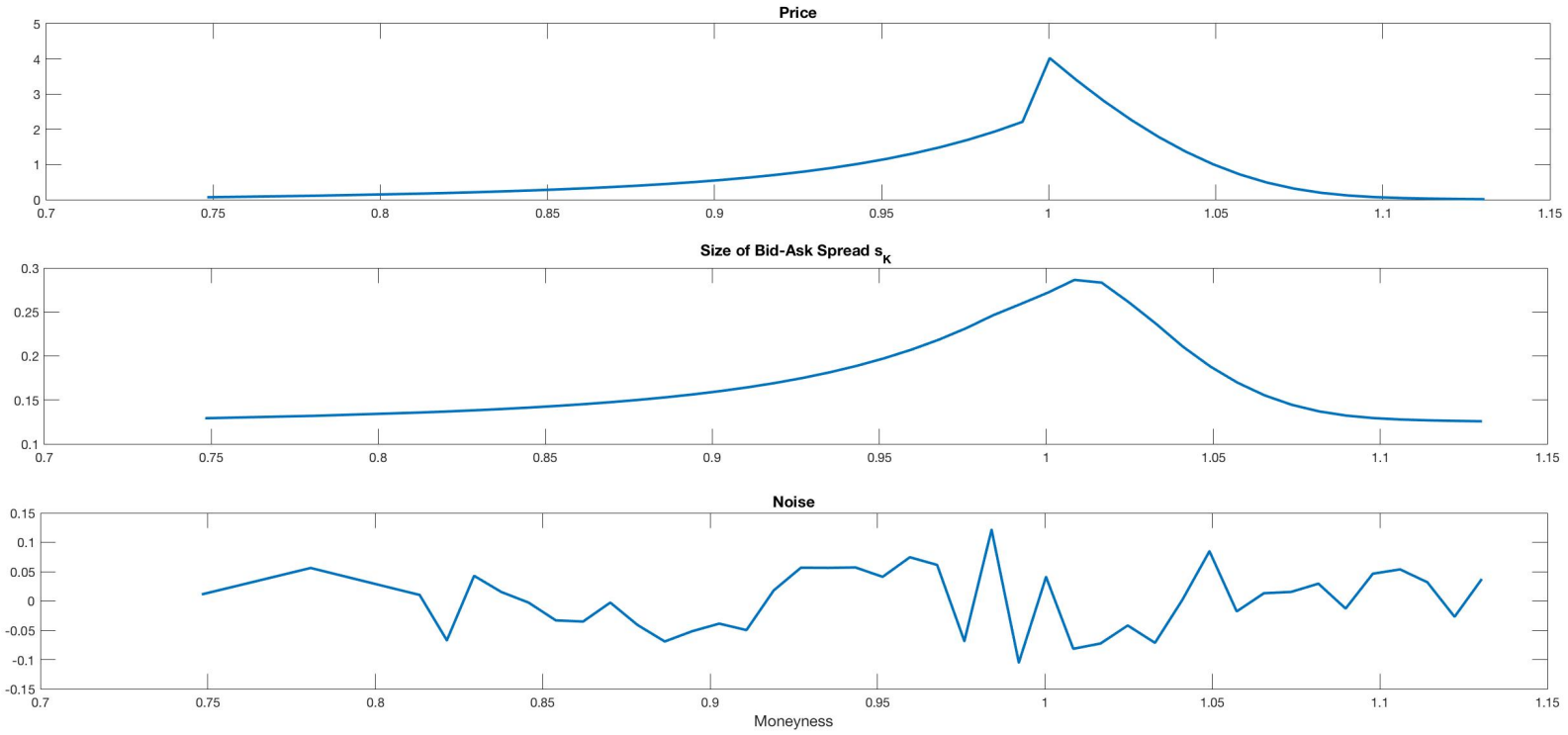

Fig. 1. **Simulated Bid-Ask Spread and Price Noise**
The figure shows an example of the OTM option prices, and the corresponding simulated bid-ask spreads and price noises.

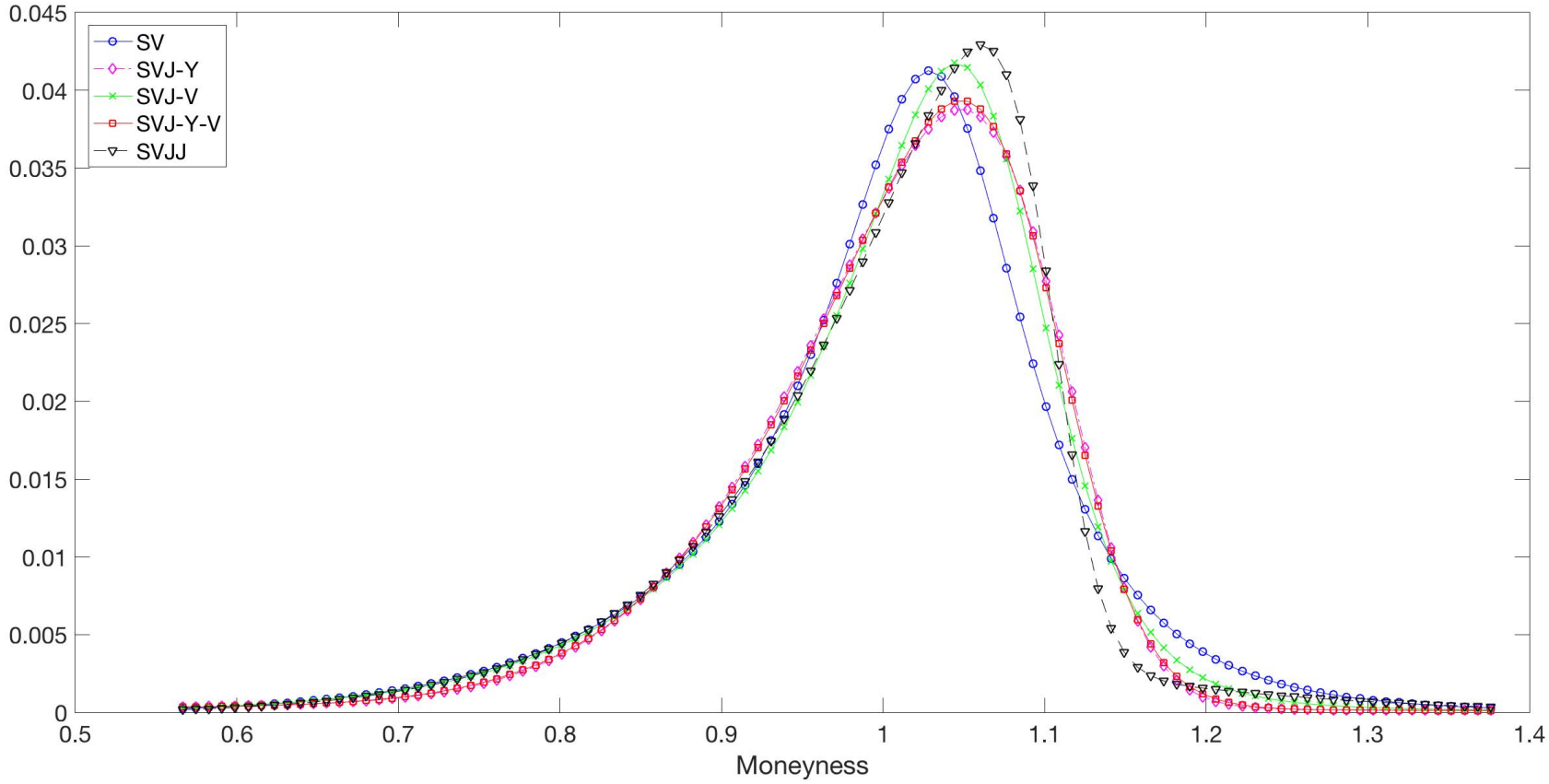

Fig. 2. **RNDs of the Affine Jump-Diffusion Models**

The figure shows RNDs of the affine jump-diffusion models. These RNDs are generated by affine jump-diffusion models by plugging the parameter estimates presented in Table 2 into Equation (8).

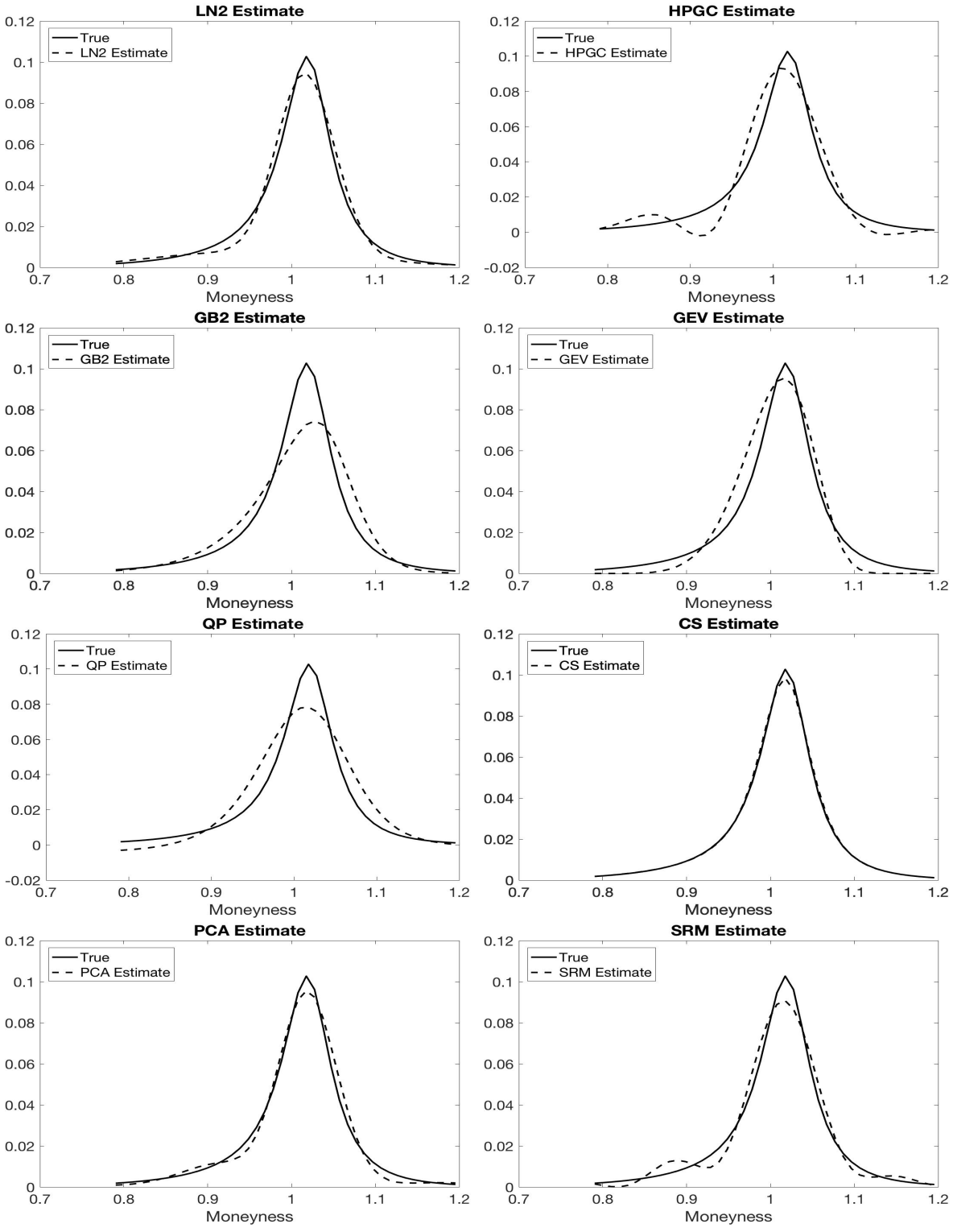

Fig. 3. **RND Estimates of the SV Model**

The figure shows RND estimates from a single round of Monte Carlo simulation under the SV model. True RNDs (solid line) are generated by the SV model with parameter estimates from Table 2 and simulated underlying index level $S_t = 101.22$, instantaneous variance level $V_t = 0.0107$, and strike price $K \in [80, 121]$; estimated RNDs (dashed lines) are extracted by eight estimation methods from the same set of artificial option data generated by the SV model perturbed by the noise perturbation process.

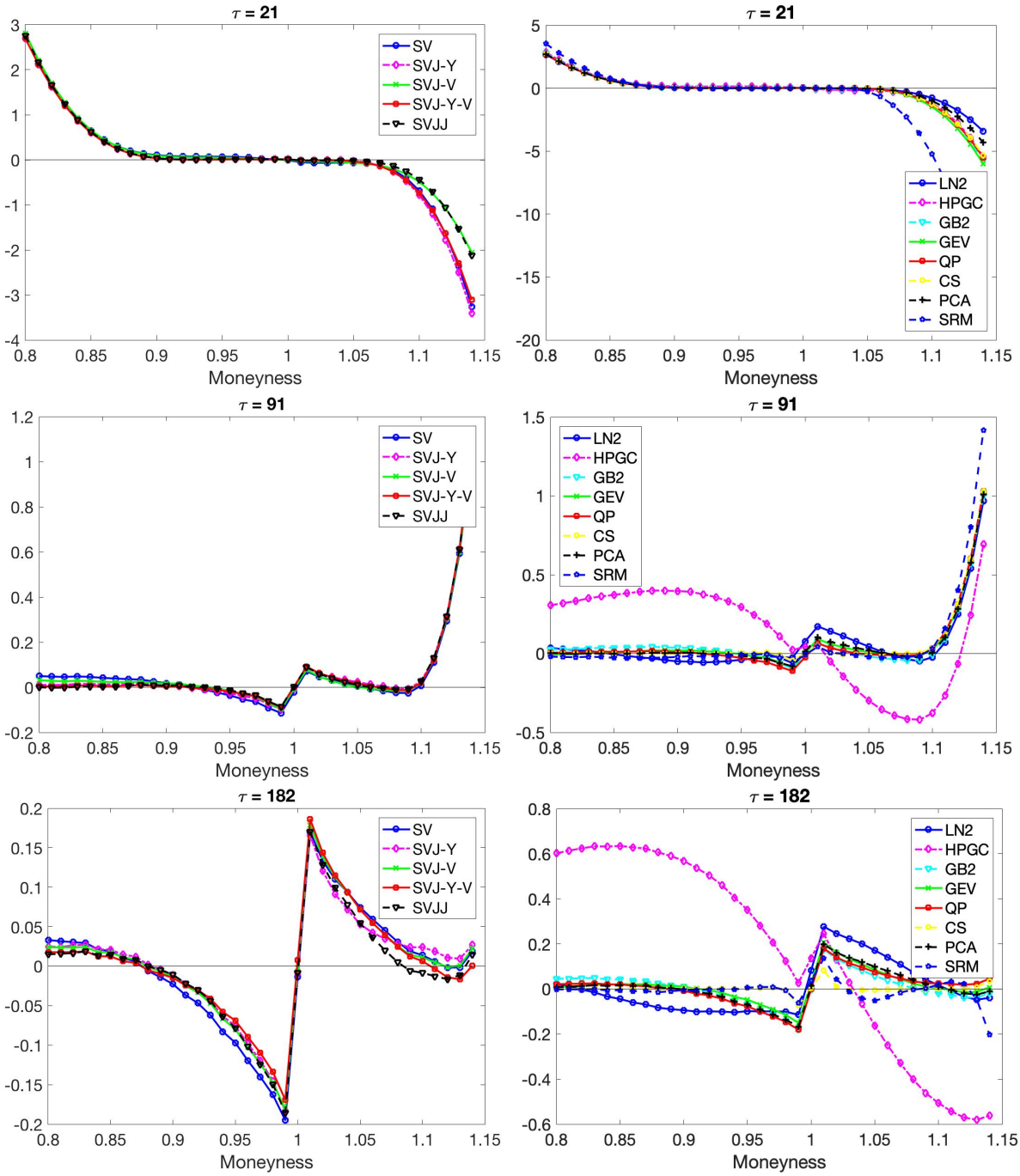

Fig. 4. **Pricing Bias Across Moneyness**

The figure shows the pricing bias of the affine jump diffusion models and estimation methods for RND across the moneyness.

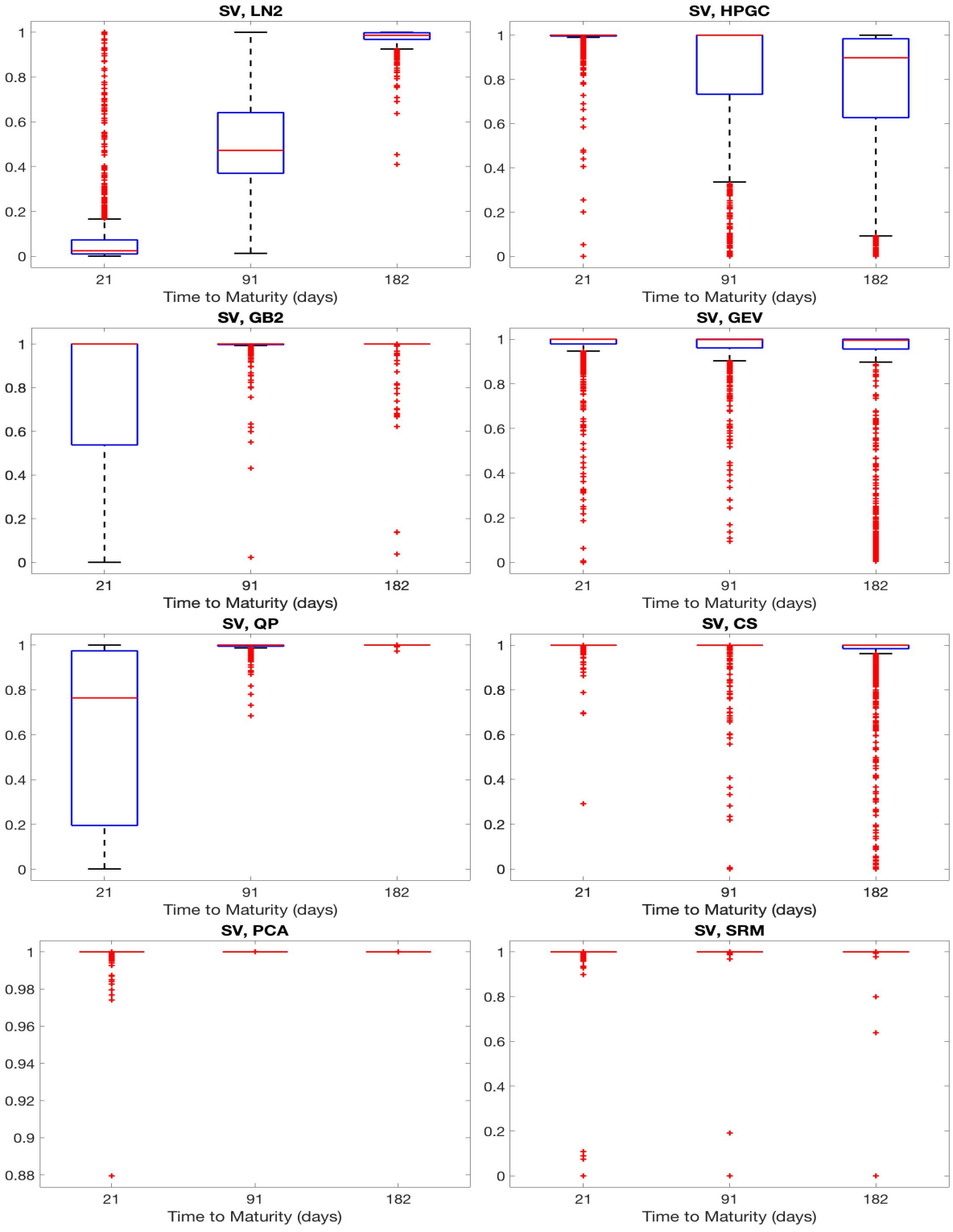

Fig. 5. **Kolmogorov-Smirnov p-values of the SV process ($\Delta K = \$1$)** The figure shows the box plot of Kolmogorov-Smirnov p-values of the SV model. The red line in each box represents the median p-value; each box covers the interquartile range of the Kolmogorov-Smirnov p-values, the upper and lower edges of the box correspond to the 25th and 75th percentiles of the p-value sample; the whiskers are marked at 1.5 times the interquartile range; outliers are plotted individually by using red "+" symbols.

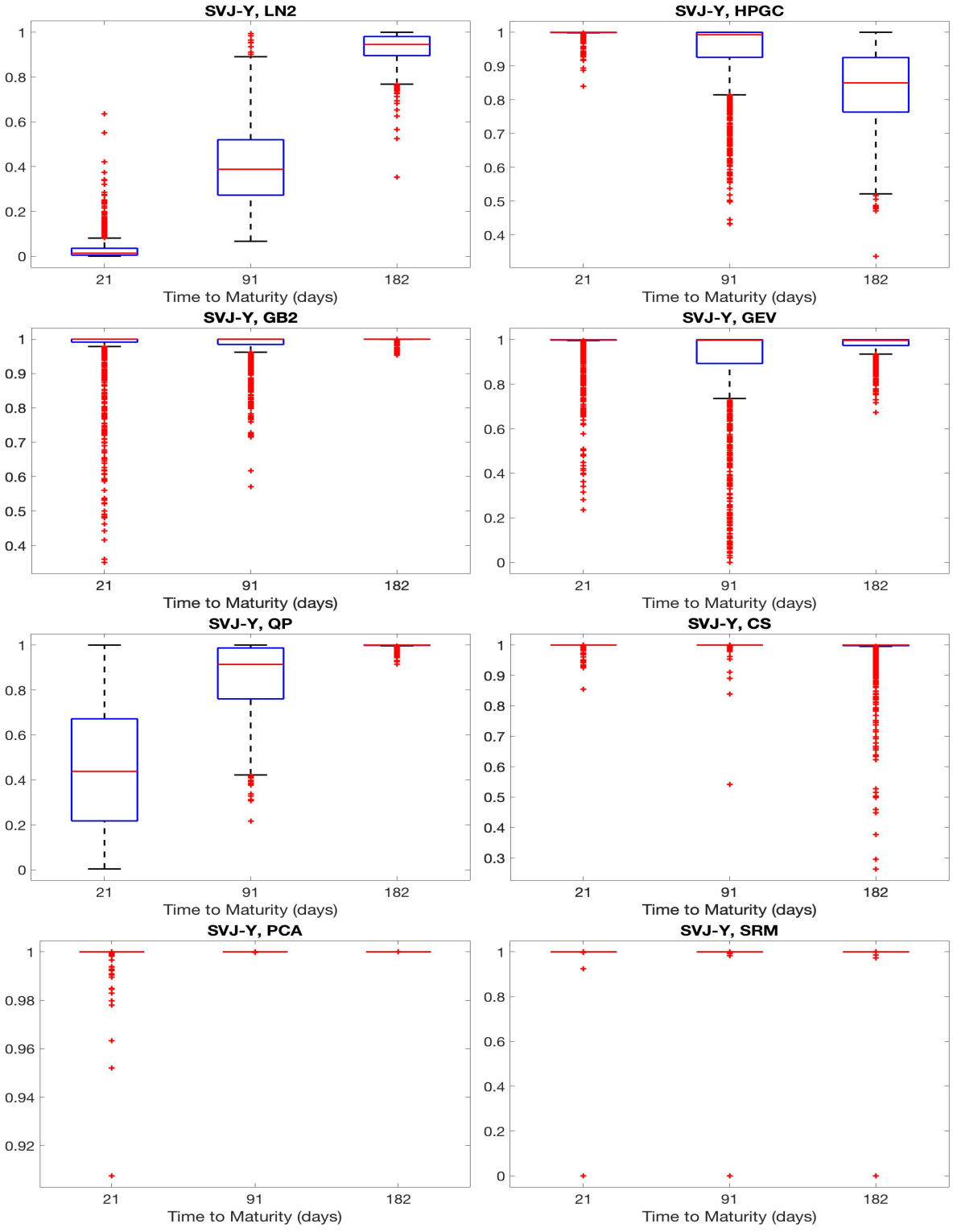

Fig. 6. **Kolmogorov-Smirnov p-values of the SVJ-Y process** ($\Delta K = \$1$) The figure shows the box plot of Kolmogorov-Smirnov p-values of the SVJ-Y model. The red line in each box represents the median p-value; each box covers the interquartile range of the Kolmogorov-Smirnov p-values, the upper and lower edges of the box correspond to the 25th and 75th percentiles of the p-value sample; the whiskers are marked at 1.5 times the interquartile range; outliers are plotted individually by using red "+" symbols.

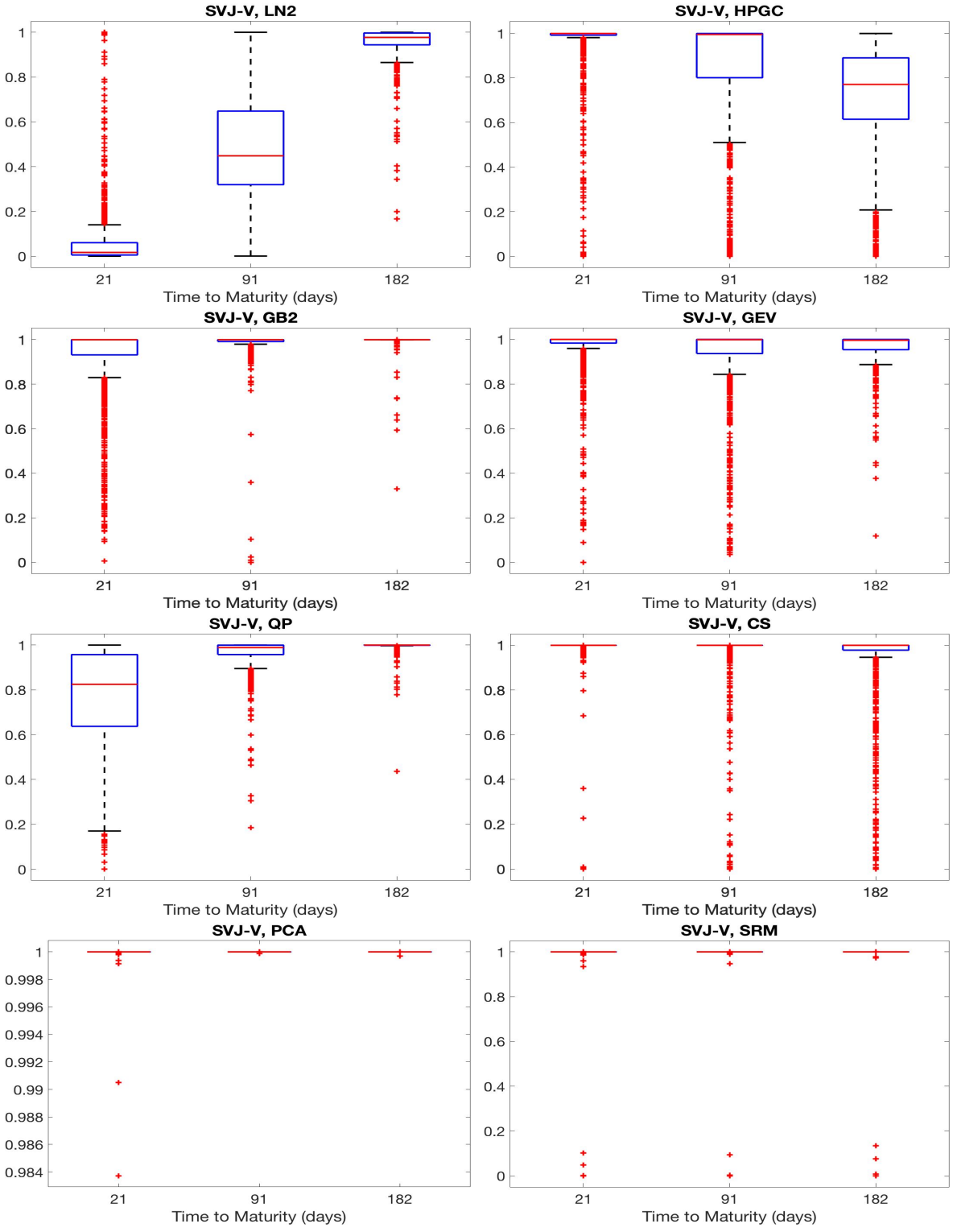

Fig. 7. **Kolmogorov-Smirnov p-values of the SVJ-V process** ($\Delta K = \$1$) The figure shows the box plot of Kolmogorov-Smirnov p-values of the SVJ-V model. The red line in each box represents the median p-value; each box covers the interquartile range of the Kolmogorov-Smirnov p-values, the upper and lower edges of the box correspond to the 25th and 75th percentiles of the p-value sample; the whiskers are marked at 1.5 times the interquartile range; outliers are plotted individually by using red "+" symbols.

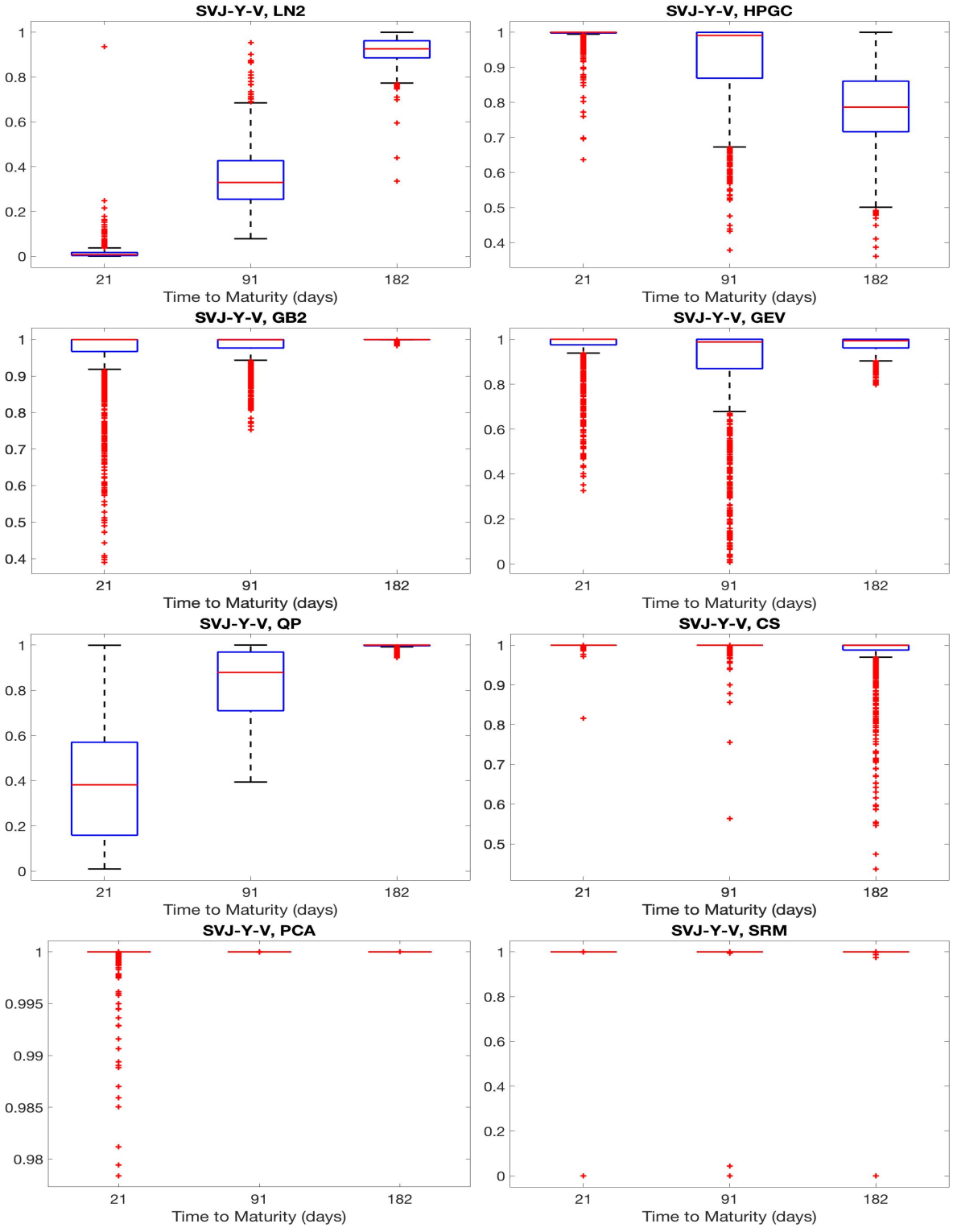

Fig. 8. **Kolmogorov-Smirnov p-values of the SVJ-Y-V process** ($\Delta K = \$1$) The figure shows the box plot of Kolmogorov-Smirnov p-values of the SVJ-Y-V model. The red line in each box represents the median p-value; each box covers the interquartile range of the Kolmogorov-Smirnov p-values, the upper and lower edges of the box correspond to the 25th and 75th percentiles of the p-value sample; the whiskers are marked at 1.5 times the interquartile range; outliers are plotted individually by using red "+" symbols.

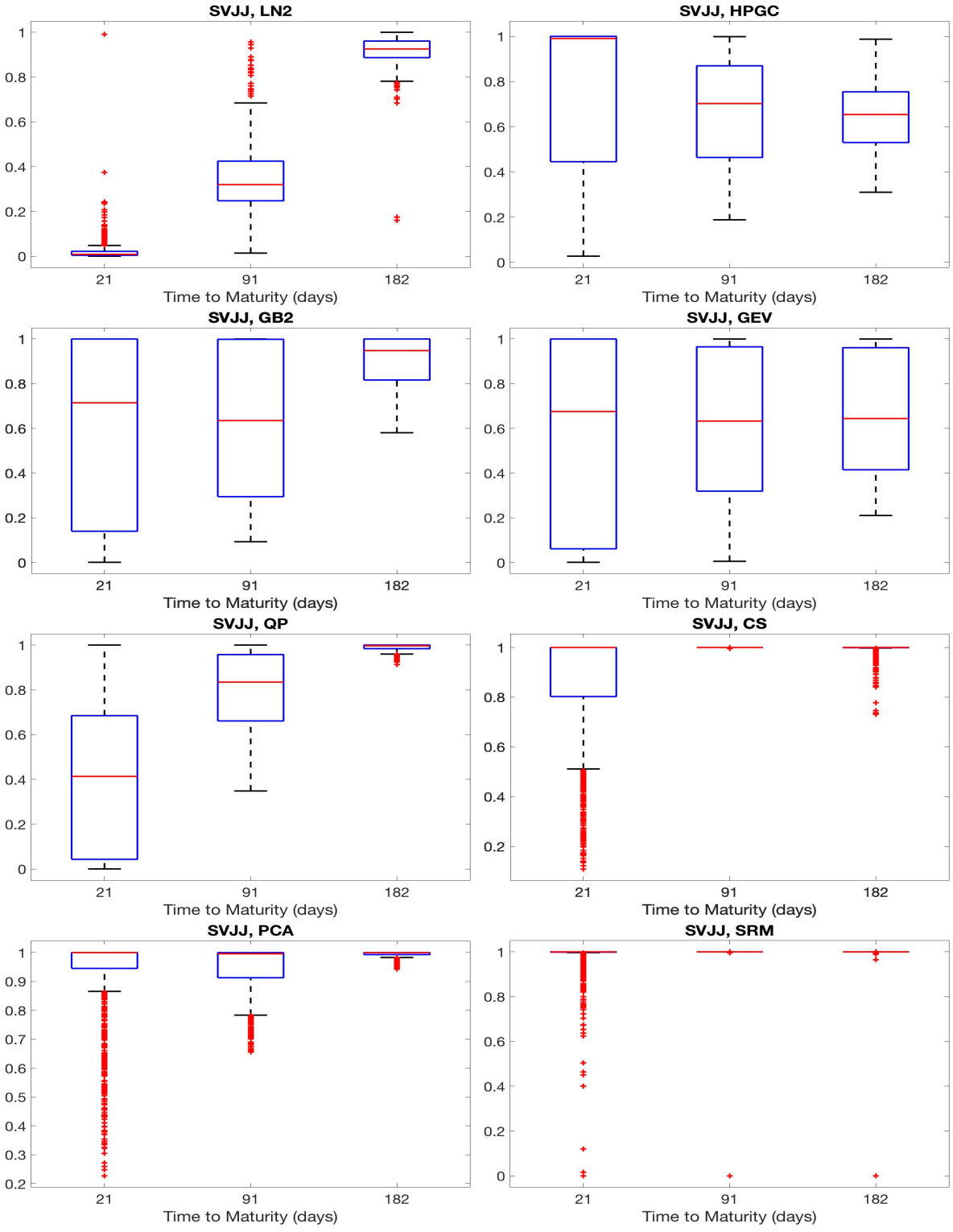

Fig. 9. **Kolmogorov-Smirnov p-values of the SVJJ process** ($\Delta K = \$1$)
The figure shows the box plot of Kolmogorov-Smirnov p-values of the SVJJ model. The red line in each box represents the median p-value; each box covers the interquartile range of the Kolmogorov-Smirnov p-values, the upper and lower edges of the box correspond to the 25th and 75th percentiles of the p-value sample; the whiskers are marked at 1.5 times the interquartile range; outliers are plotted individually by using red "+" symbols.

Supplementary Data

Table 7: **Summary Statistics of p-values of the Kolmogorov-Smirnov Test ($\Delta K = \$5$)**

	$\tau = 21$			$\tau = 91$			$\tau = 182$		
	Average p-value	Standard Deviation	Rejection of H_0 (%)	Average p-value	Standard Deviation	Rejection of H_0 (%)	Average p-value	Standard Deviation	Rejection of H_0 (%)
SV process									
LN2	0.09	0.20	72.9	0.52	0.22	0.2	0.97	0.04	0.0
HPGC	0.94	0.14	0.1	0.84	0.27	1.8	0.75	0.31	4.8
GB2	0.79	0.30	0.3	0.99	0.02	0.0	1.00	0.01	0.0
GEV	0.95	0.11	0.0	0.97	0.06	0.0	0.98	0.05	0.1
QP	0.58	0.38	17.0	0.99	0.03	0.0	1.00	0.00	0.0
CS	0.94	0.15	0.0	0.99	0.06	0.1	0.98	0.11	0.4
PCA	0.98	0.07	0.0	1.00	0.00	0.0	1.00	0.00	0.0
SRM	0.89	0.23	4.2	0.97	0.16	2.1	0.97	0.17	2.8
SVJ-Y process									
LN2	0.06	0.17	77.3	0.43	0.19	0.4	0.94	0.07	0.0
HPGC	0.99	0.07	0.0	0.94	0.11	0.0	0.84	0.11	0.0
GB2	0.95	0.12	0.0	0.97	0.06	0.0	1.00	0.01	0.0
GEV	0.96	0.12	0.0	0.97	0.06	0.0	0.97	0.05	0.0
QP	0.54	0.27	0.8	0.89	0.13	0.0	1.00	0.01	0.0
CS	0.98	0.06	0.0	1.00	0.00	0.0	1.00	0.02	0.0
PCA	1.00	0.01	0.0	1.00	0.00	0.0	1.00	0.00	0.0
SRM	0.95	0.20	3.5	0.98	0.14	1.8	0.98	0.14	2.1
SVJ-V process									
LN2	0.11	0.23	69.6	0.50	0.24	1.0	0.95	0.08	0.0
HPGC	0.93	0.17	0.6	0.84	0.27	3.7	0.70	0.26	4.7
GB2	0.91	0.17	0.1	0.98	0.06	0.1	1.00	0.02	0.0
GEV	0.96	0.11	0.2	0.95	0.10	0.1	0.96	0.08	0.1
QP	0.69	0.28	1.0	0.97	0.06	0.0	1.00	0.02	0.0
CS	0.97	0.10	0.1	0.98	0.10	0.2	0.97	0.13	0.5
PCA	0.99	0.06	0.0	1.00	0.00	0.0	1.00	0.00	0.0
SRM	0.93	0.19	2.6	0.97	0.15	2.3	0.98	0.15	2.3
SVJ-Y-V process									
LN2	0.04	0.16	89.2	0.36	0.15	0.2	0.93	0.06	0.0
HPGC	0.99	0.06	0.0	0.92	0.13	0.0	0.79	0.11	0.0
GB2	0.94	0.13	0.0	0.97	0.05	0.0	1.00	0.01	0.0
GEV	0.95	0.13	0.0	0.96	0.06	0.0	0.97	0.04	0.0
QP	0.49	0.24	0.6	0.87	0.13	0.0	1.00	0.01	0.0
CS	0.99	0.04	0.0	1.00	0.00	0.0	1.00	0.01	0.0
PCA	1.00	0.02	0.0	1.00	0.00	0.0	1.00	0.00	0.0
SRM	0.95	0.20	3.6	0.98	0.14	1.8	0.98	0.14	2.0
SVJJ process									
LN2	0.07	0.20	82.4	0.36	0.19	0.9	0.91	0.08	0.0
HPGC	0.74	0.35	4.7	0.65	0.23	0.0	0.64	0.15	0.0
GB2	0.58	0.41	14.5	0.59	0.34	0.0	0.85	0.14	0.0
GEV	0.57	0.43	22.3	0.49	0.39	9.3	0.66	0.26	0.0
QP	0.42	0.35	28.4	0.79	0.21	0.0	0.99	0.02	0.0
CS	0.75	0.34	2.7	1.00	0.02	0.0	1.00	0.00	0.0
PCA	0.83	0.28	0.3	0.93	0.09	0.0	0.99	0.01	0.0
SRM	0.78	0.32	5.0	0.96	0.18	3.1	0.96	0.18	3.3

Notes: The table reports the mean and the standard deviation of p-values of the Kolmogorov-Smirnov test of the estimation performance of methods for RND. The standard deviation of p-values is computed from a set of 1000 RND estimates; the rejection rate is the percentage of density estimates rejected at 5% significance level, and is calculated by dividing the number of p-values smaller than 0.05 by the total number of p-values (which is 1000).

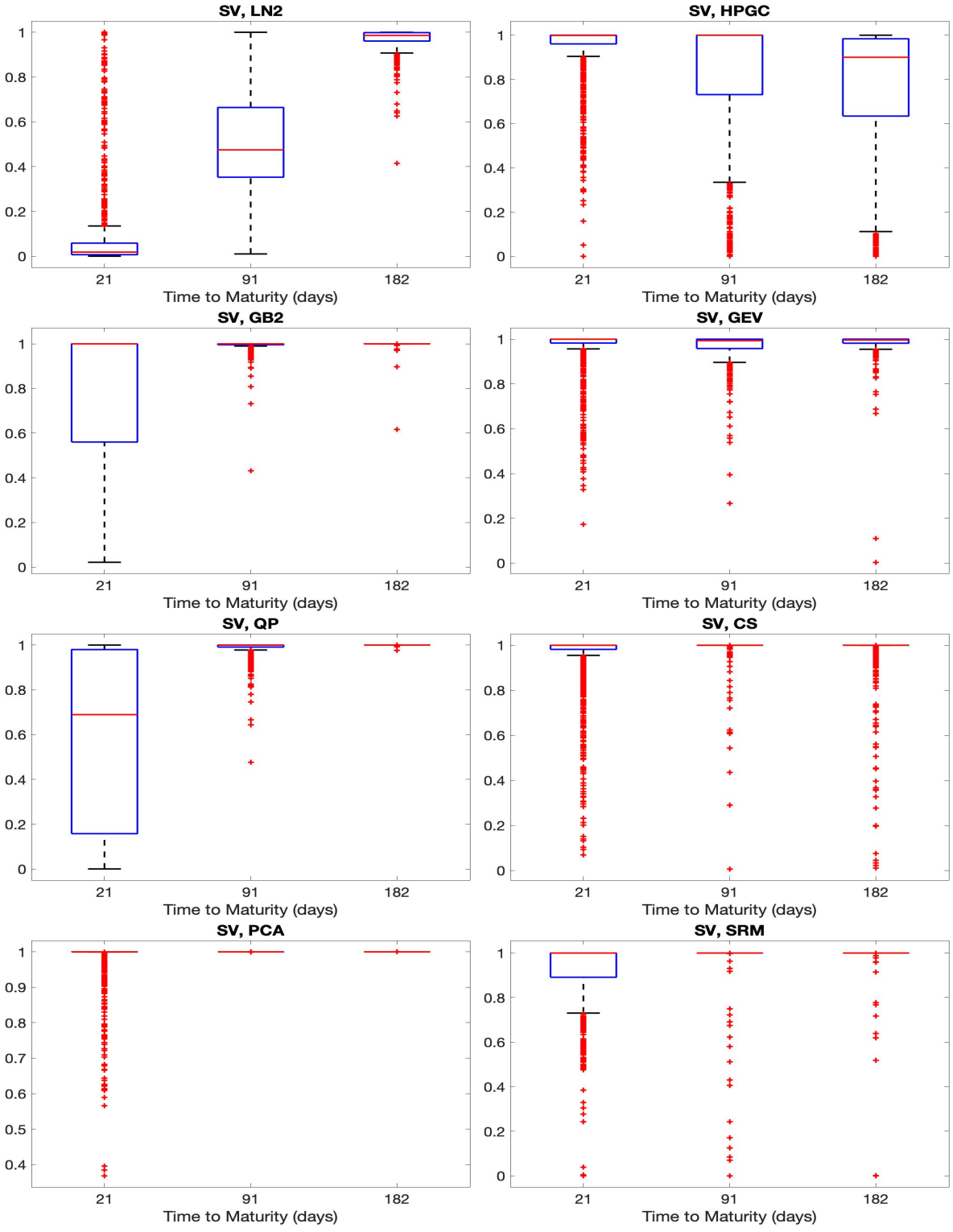

Fig. 10. **Kolmogorov-Smirnov p-values of the SV process** ($\Delta K = \$5$)
The figure shows the box plot of Kolmogorov-Smirnov p-values of the SV model. The red line in each box represents the median p-value; each box covers the interquartile range of the Kolmogorov-Smirnov p-values, the upper and lower edges of the box correspond to the 25th and 75th percentiles of the p-value sample; the whiskers are marked at 1.5 times the interquartile range; outliers are plotted individually by using red "+" symbols.

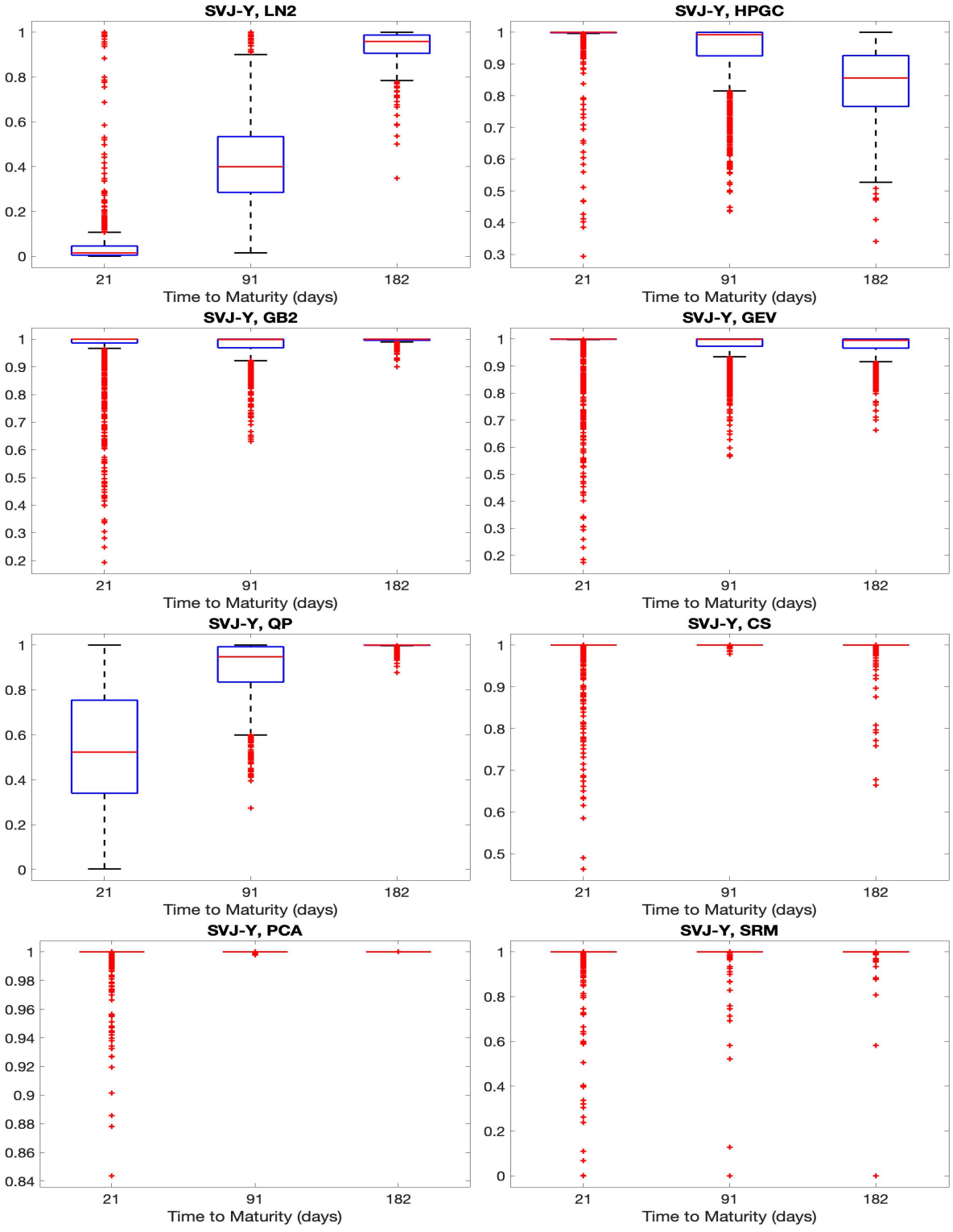

Fig. 11. **Kolmogorov-Smirnov p-values of the SVJ-Y process** ($\Delta K = \$5$) The figure shows the box plot of Kolmogorov-Smirnov p-values of the SVJ-Y model. The red line in each box represents the median p-value; each box covers the interquartile range of the Kolmogorov-Smirnov p-values, the upper and lower edges of the box correspond to the 25th and 75th percentiles of the p-value sample; the whiskers are marked at 1.5 times the interquartile range; outliers are plotted individually by using red "+" symbols.

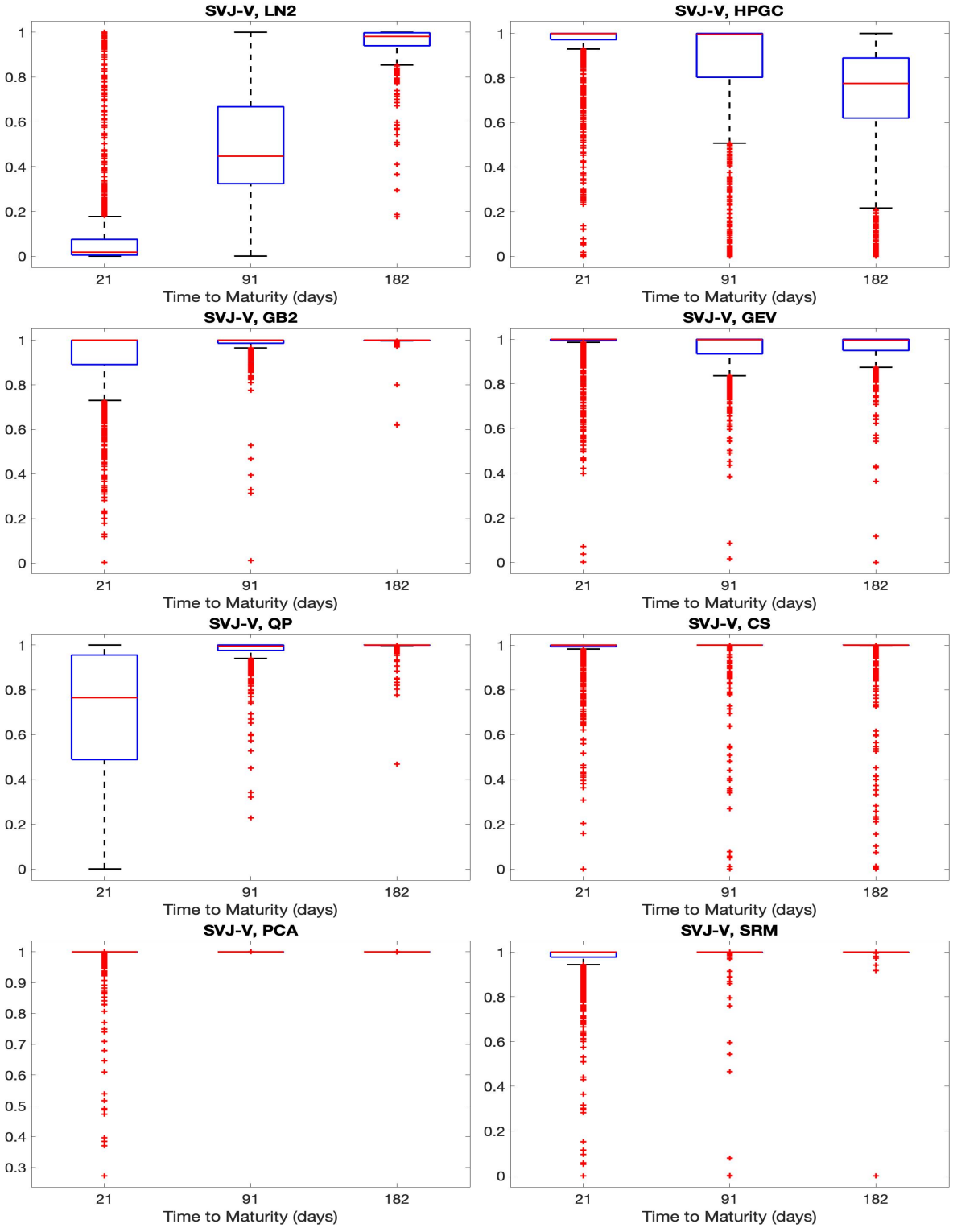

Fig. 12. **Kolmogorov-Smirnov p-values of the SVJ-V process** ($\Delta K = \$5$) The figure shows the box plot of Kolmogorov-Smirnov p-values of the SVJ-V model. The red line in each box represents the median p-value; each box covers the interquartile range of the Kolmogorov-Smirnov p-values, the upper and lower edges of the box correspond to the 25th and 75th percentiles of the p-value sample; the whiskers are marked at 1.5 times the interquartile range; outliers are plotted individually by using red "+" symbols.

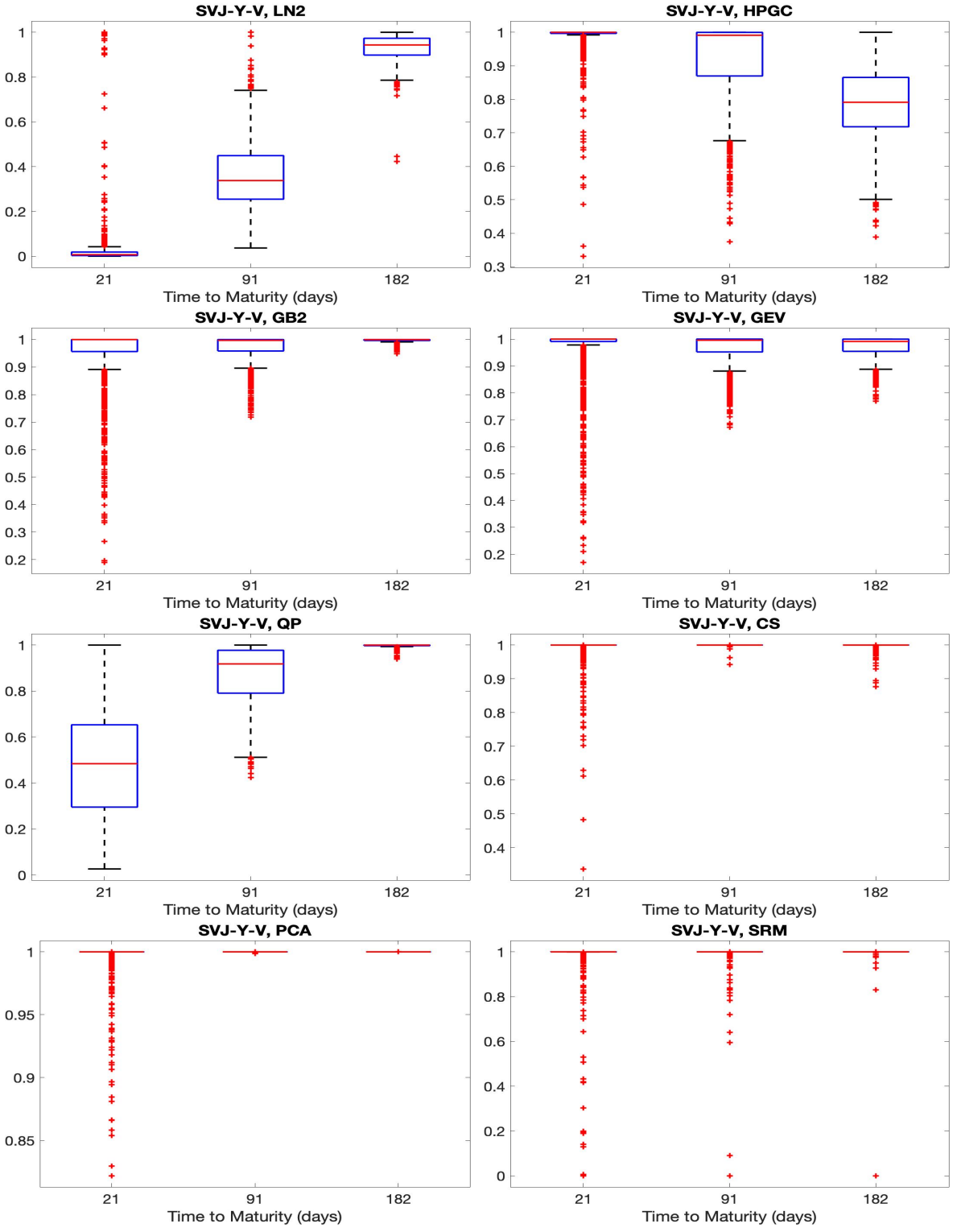

Fig. 13. **Kolmogorov-Smirnov p-values of the SVJ-Y-V process** ($\Delta K = \$5$) The figure shows the box plot of Kolmogorov-Smirnov p-values of the SVJ-Y-V model. The red line in each box represents the median p-value; each box covers the interquartile range of the Kolmogorov-Smirnov p-values, the upper and lower edges of the box correspond to the 25th and 75th percentiles of the p-value sample; the whiskers are marked at 1.5 times the interquartile range; outliers are plotted individually by using red "+" symbols.

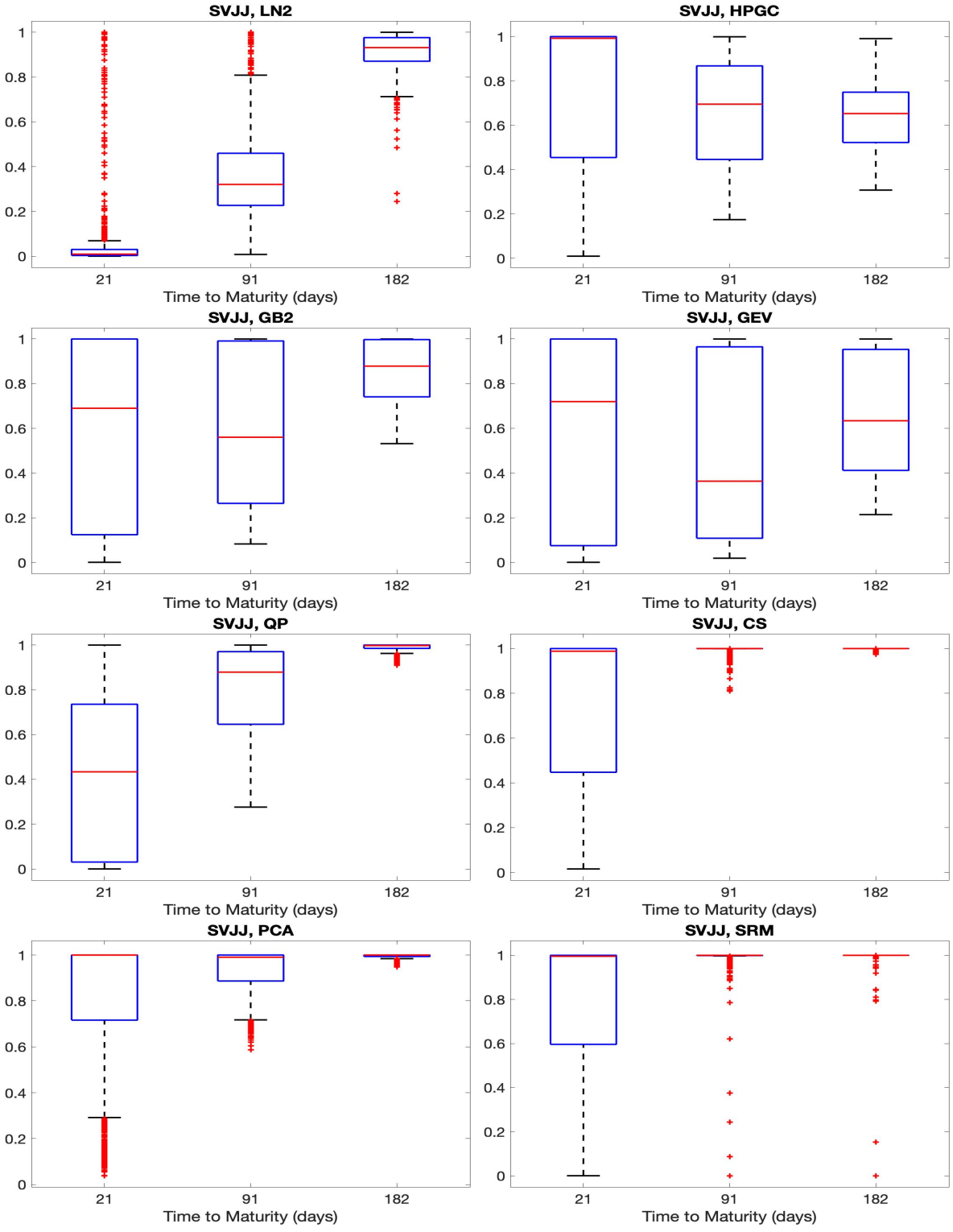

Fig. 14. **Kolmogorov-Smirnov p-values of the SVJJ process** ($\Delta K = \$5$) The figure shows the box plot of Kolmogorov-Smirnov p-values of the SVJJ model. The red line in each box represents the median p-value; each box covers the interquartile range of the Kolmogorov-Smirnov p-values, the upper and lower edges of the box correspond to the 25th and 75th percentiles of the p-value sample; the whiskers are marked at 1.5 times the interquartile range; outliers are plotted individually by using red "+" symbols.